CT-930-551
Dow-2016

CM

Centro de Investigación y de Estudios Avanzados
del Instituto Politécnico Nacional
Unidad Guadalajara

Reducción de Orden de Aproximaciones Racionales para Análisis de Transitorios Electromagnéticos Utilizando Descomposición en Valores Singulares

Tesis que presenta:
Edgar Yitzhak Medina Lara

para obtener el grado de:
Maestro en ciencias

en la especialidad de:
Ingeniería Eléctrica

Director de Tesis:
Dr. Amner Israel Ramírez Vázquez

CINVESTAV del IPN Unidad Guadalajara, Guadalajara, Jalisco, Octubre de 2015

Centro de Investigación y de Estudios Avanzados
del Instituto Politécnico Nacional
Unidad Guadalajara

Singular Value Decomposition-based Reduced-Order Rational Approximation for Electromagnetic Transient Analysis

A thesis presented by·
Edgar Yitzhak Medina Lara

to obtain the degree of:
Master of Science

in the subject of:
Electrical Engineering

Thesis Advisor:
Dr. Amner Israel Ramírez Vázquez

CINVESTAV del IPN Unidad Guadalajara, Guadalajara, Jalisco, October 2015

Reducción de Orden de Aproximaciones Racionales para Análisis de Transitorios Electromagnéticos Utilizando Descomposición en Valores Singulares

Tesis de Maestría en Ciencias
Ingeniería Eléctrica

Por:
Edgar Yitzhak Medina Lara
Ingeniero en Electricidad y Automatización
Universidad Autónoma de San Luis Potosí 2006-2011

Becario de CONACYT, expediente no. 300973

Director de Tesis:
Dr. Amner Israel Ramírez Vázquez

CINVESTAV del IPN Unidad Guadalajara, Octubre de 2015.

Singular Value Decomposition-based Reduced-Order Rational Approximation for Electromagnetic Transient Analysis

Master of Science Thesis
In Electrical Engineering

By:

Edgar Yitzhak Medina Lara

Electrical and Automation Engineer

Universidad Autónoma de San Luis Potosí 2006-2011

Scholarship granted by CONACYT, No. 300973

Thesis Advisor:

Dr. Amner Israel Ramírez Vázquez

CINVESTAV del IPN Unidad Guadalajara, October 2015.

ACKNOWLEDGMENTS

I would like to thank to:

My parents, Antero and Manuela, for giving me all their unconditional support, comprehension, and love.

My brothers and sisters, Sheila, Omar, Gaby, and Deya.

My advisor, Dr. Abner Ramirez, for his patience, guidance, and for offering me his great support and knowledge.

My friends at CINVESTAV.

Conacyt, for the granted scholarship.

INDEX

LIST OF FIGURES

LIST OF TABLES

RESUMEN

Esta tesis presenta una técnica de reducción de orden de modelos (MOR, por sus siglas en inglés) basada en descomposición en valores singulares (SVD) y enfocada al análisis de transitorios electromagnéticos. El método propuesto adopta inicialmente la aproximación racional de una función dependiente de la frecuencia, expresada como un conjunto de fracciones parciales, obtenida a través de vector fitting (VF) para un rango amplio de frecuencias. Subsecuentemente, la metodología propuesta aplica un truncamiento basado en SVD a la aproximación obtenida por VF en bajas frecuencias, resultando en una aproximación de orden reducido para bajas frecuencias. Para el rango de altas frecuencias, el truncamiento basado en SVD es aplicado al error obtenido al comparar la aproximación original de VF y la aproximación de orden reducido para bajas frecuencias. Finalmente, las aproximaciones resultantes son conjuntadas para la solución de transitorios electromagnéticos. El modelo de orden reducido obtenido logra disminuir el uso de recursos computacionales, comparado con el sistema original dado por VF, sin perder precisión. Se presentan dos ejemplos ilustrativos se presentan para validar el método propuesto.

ABSTRACT

This thesis presents a model order reduction (MOR) technique, based on singular value decomposition (SVD), aimed to electromagnetic transient (EMT) analysis. The proposed method initially adopts a rational approximation of a frequency-dependent function, expressed as a set of partial fractions and obtained by the vector fitting (VF) software tool for a wide frequency range. Subsequently, the method applies SVD-based truncation to the approximation given by VF in the low-frequency (LF) range, resulting in a LF reduced-order approximation. Then, the SVD-based truncation is applied to the error obtained by comparing the VF function and the LF approximation in the high-frequency (HF) range. Finally, the resultant LF and HF reduced-order approximations are assembled for EMT solution. The obtained reduced-order model achieves computational savings compared to the original full-size system given by VF without losing accuracy. Two illustrative examples are presented to validate the proposed method.

1 INTRODUCTION

1.1 Use of rational approximations for electromagnetic transient (EMT) analysis

Rational approximations, represented by a set of partial fractions, are commonly used for the modeling and simulation of electrical networks and/or individual elements such as transmission lines and transformers [1-4]. The fact that a rational approximation can be expressed as a state-space formulation makes attractive to employ model order reduction (MOR) techniques to optimize the dimensions of the state-space system of the model under analysis.

Due to different dynamics involved in an electrical phenomenon, wide-band models that cover from few Hertz to several thousands of Hertz are employed. In fact, most of the existent MOR techniques consider by default a wide frequency range [4]. However, there are cases in which a narrow frequency bandwidth has the most impact on the phenomenon under analysis. Recently, frequency-domain MOR methods have been developed to represent a system via a reduced-order model accurate within a specific frequency bandwidth [5-8]. Therefore, a rational approximation can be obtained for EMT analysis and reduced either to represent wide frequency-range phenomena or to focus on specific frequency-range via a subset of poles.

1.2 Problem statement

Conventional rational fitting software tools have as input an arbitrary range of frequencies pre-specified by the user. Also, the order of the rational approximation is typically adjusted by a trial-error procedure to comply with an acceptable approximation error. There have been some proposals on the order of rational approximation for a given approximation error [9,10]; however, rigorously speaking, no precise criterion exists. Moreover, traditional fitting methods are prompted to generate out-of-band poles for which an elimination scheme is required; otherwise, a spurious oscillatory phenomenon may appear in the EMT simulation [11].

1.3 Thesis objective

This thesis proposes a practical and effective MOR technique based on direct application of singular value decomposition (SVD) and valid on an arbitrarily wide frequency bandwidth. The proposed method has as starting system the set of poles (equivalently, partial fractions) obtained by the vector fitting (VF) [1] software tool, and obtains two subsets of poles, via SVD truncation, corresponding to low- and high-frequency sub-bands. The two subsets of poles (alternatively, partial fractions) are then assembled for EMT simulation in the form of state-space realizations.

2 VECTOR FITTING AND STATE-SPACE REALIZATIONS

2.1 Description of VF

VF is a numerical tool aimed to approximate, via rational functions, calculated or measured frequency response of a given network. VF is widely used, mainly in the power systems area, due to its accuracy and robustness [1,11,12]. A brief description of VF is presented in this section.

A rational (scalar) function approximation of order n can be expressed as the sum of partial fractions:

$$f(s) = \sum_{k=1}^{n} \frac{c_k}{s - p_k} + d + sh, \tag{2.1}$$

where c_k and p_k are residues and poles, respectively; d and h represent real constant terms.

The problem is to estimate (c_k, p_k, d, h) in (2.1). To achieve this, (2.1) is evaluated using N frequency samples within a given frequency bandwidth and the resulting system is solved as a linear problem in two steps as described next.

Step1. Pole identification

An arbitrary set of poles $\bar{a}_k$ is initially proposed, and f(s) is multiplied by an unknown function $\sigma(s)$, leading to

$$\sigma(s) f(s) = \sum_{k=1}^{n} \frac{c_k}{s - \bar{a}_k} + d + sh. \tag{2.2}$$

In addition, the unknown function $\sigma(s)$ is represented by a rational approximation of the type

$$\sigma(s) = \sum_{k=1}^{n} \frac{\tilde{c}_k}{s - \bar{a}_k} + 1. \tag{2.3}$$

The function $\sigma(s)$ is required to satisfy the condition that the poles of both $\sigma(s)$ and $\sigma(s)f(s)$ are the same. Multiplying (2.3) by $f(s)$ and matching with (2.2) results in:

$$\left(\sum_{k=1}^{n}\frac{c_k}{s-\bar{a}_k}+d+sh\right)=\left(\sum_{n=1}^{N}\frac{\tilde{c}_k}{s-\bar{a}_k}+1\right)f(s), \tag{2.4}$$

or, in compact form

$$(\sigma f)_{fit}(s)=\sigma_{fit}(s)f(s). \tag{2.5}$$

Also, (2.4) can be rewritten as [1]

$$\left(\sum_{k=1}^{n}\frac{c_k}{s-\bar{a}_k}+d+sh\right)-\left(\sum_{k=1}^{n}\frac{\tilde{c}_k}{s-\bar{a}_k}\right)f(s)=f(s). \tag{2.6}$$

Then, evaluating (2.6) for a specific frequency point l, we obtain

$$A_l x=b_l, \tag{2.7}$$

where:

$$A_l=\left[\frac{1}{s_l-a_1}, \quad \cdots, \quad \frac{1}{s_l-a_N}, \quad 1, \quad s_l, \quad \frac{-f(s_l)}{s_l-a_1}, \quad \cdots, \quad \frac{-f(s_l)}{s_l-a_N}\right], \tag{2.8a}$$

$$x=[c_1, \ \cdots, \ c_N, \ d, \ h, \ \tilde{c}_1, \ \cdots, \ \tilde{c}_N]^T \tag{2.8b}$$

where T denotes transposed.

$$b_l=f(s_l). \tag{2.8c}$$

Evaluating (2.8a) and (2.8c) for N points results in the following over-determined linear matrix equation:

$$Ax=b. \tag{2.9}$$

Finally, (2.9) is solved as a least squares problem.

Each term within parenthesis in (2.4) can be expressed as:

$$(\sigma f)_{fit}(s)=h\frac{\prod_{k=1}^{n+1}(s-z_k)}{\prod_{k=1}^{n}(s-\bar{a}_k)}, \qquad \sigma_{fit}(s)=\frac{\prod_{k=1}^{n}(s-\tilde{z}_k)}{\prod_{k=1}^{n}(s-\bar{a}_k)} \tag{2.10}$$

From (2.10) we obtain the following expression for $f(s)$

$$f(s)=\frac{(\sigma f)_{fit}(s)}{\sigma_{fit}(s)}=h\frac{\prod_{k=1}^{n+1}(s-z_k)}{\prod_{k=1}^{n}(s-\tilde{z}_k)} \tag{2.11}$$

It can be noticed in (2.11) that the poles of $f(s)$ correspond to the zeros of $\sigma_{fit}(s)$. Hence, solving (2.9) provides a set of zeros of $\sigma_{fit}(s)$, and according to (2.11), the new set of poles corresponding to $f(s)$ are obtained. It is noted that solution of (2.9) can produce unstable poles; this problem is solved in practical implementations by inverting the sign of the real part of the unstable poles [1].

Step2. Residue identification

After calculating the poles of $f(s)$, its corresponding zeros are calculated as the eigenvalues of

$$H = A - b\tilde{c}^T \tag{2.12}$$

where A is a diagonal matrix containing the arbitrary starting poles, b represents a column vector consisting of "ones", and $\tilde{c}^T$ is a row vector composed by the residues of $\sigma_{fit}(s)$.

The outlined procedure has been generalized and implemented into the VF software tool for the case of a frequency-dependent matrix $F(s)$.

2.2 Matrix rational approximations and state-space realizations

In the general multi-input multi-output (MIMO) case, a transfer function evaluated for a given bandwidth is assumed to be available as a frequency-dependent matrix $F(s)$.

Based on the theory presented in section 2.1 for a scalar function, $F(s)$, of size $m \times m$ can be readily approximated via VF with all of its elements sharing a common set of poles [1, 13]. The resultant rational approximation, assumed of order n, can be expressed as a state-space formulation as follows [13]:

$$\begin{aligned} \dot{x} &= Ax + Bu \\ y &= Cx + Du \end{aligned} \tag{2.13}$$

The state-space system, as in (2.13), can be used for EMT simulation or for MOR purposes. Matrices A, B, C and D, for the multiphase case, are structured as follows:

$$A = diag\left\{p_1, \ p_2, \ \cdots, \ p_n, \ p_1, \ p_2, \ \cdots, \ p_n, \ \cdots, \ p_1, \ p_2, \ \cdots, \ p_n\right\}, \tag{2.14a}$$

$$B = \begin{bmatrix} 1 & 1 & \cdots & 1 & 0 & 0 & \cdots & 0 & \cdots & 0 & 0 & \cdots & 0 \\ 0 & 0 & \cdots & 0 & 1 & 1 & \cdots & 1 & \cdots & 0 & 0 & \cdots & 0 \\ \vdots & \vdots & & \vdots & \vdots & \vdots & & \vdots & & \vdots & \vdots & & \vdots \\ 0 & 0 & \cdots & 0 & 0 & 0 & \cdots & 0 & \cdots & 1 & 1 & \cdots & 1 \end{bmatrix}^T \tag{2.14b}$$

$$C = \begin{bmatrix} c_{1,1,1} & c_{1,1,2} & \cdots & c_{1,1,n} & c_{121} & c_{1,2,2} & \cdots & c_{1,2,n} & \cdots & c_{1,m,1} & c_{1,m,2} & \cdots & c_{1,m,n} \\ c_{2,1,1} & c_{2,1,2} & \cdots & c_{2,1,n} & c_{221} & c_{2,2,2} & \cdots & c_{2,2,n} & \cdots & c_{2,m,1} & c_{2,m,2} & \cdots & c_{2,m,n} \\ \vdots & \vdots & & \vdots & \vdots & \vdots & & \vdots & & \vdots & \vdots & & \vdots \\ c_{m,1,1} & c_{m,1,2} & \cdots & c_{m,1,n} & c_{m21} & c_{m,2,2} & \cdots & c_{m,2,n} & \cdots & c_{m,m,1} & c_{m,m,2} & \cdots & c_{m,m,n} \end{bmatrix}, \tag{2.14c}$$

$$D = \begin{bmatrix} d_{1,1} & d_{1,2} & \cdots & d_{1,m} \\ d_{2,1} & d_{2,2} & \cdots & d_{2,m} \\ \vdots & \vdots & & \vdots \\ d_{m,1} & d_{m,2} & \cdots & d_{m,m} \end{bmatrix}. \tag{2.14d}$$

In (2.14), A, B, C, and D are of dimensions $(m\times n)\times(m\times n)$, $(m\times n)\times m$, $m\times(m\times n)$, and $m\times m$, respectively. Expression (2.14a) shows that, for matrix A, the common set of poles is repeated m times. Similarly, a row vector containing m "ones" is repeated in matrix B, as shown in (2.14b). Also, in (2.14c) $c_{i,j,k}$ represents the (i^{th}, j^{th}) element of the residue matrix corresponding to the k^{th} pole.

Based on (2.14), the matrix structure for the scalar case becomes:

$$A = diag\ \{p_1,\ p_2,\ \cdots,\ p_n\}, \tag{2.15a}$$

$$B = [1,\ 1,\ \cdots,\ 1]^T \tag{2.15b}$$

$$C = [c_1,\ c_2,\ \cdots.\ c_n], \tag{2.15c}$$

and D represents a constant term.

2.3 Conclusions

The fundamentals of the VF software tool have been presented. Also, it has been stated that VF can approximate both scalar functions and frequency-dependent matrices. Finally, the conversion of rational approximations to state-space formulation is outlined.

3 SVD APPLIED TO A FITTED FUNCTION IN A SPECIFIC FREQUENCY RANGE

In this Chapter, the proposed SVD-based MOR technique, applied to a rational approximation in a specific frequency bandwidth, is described [14].

3.1 Solution scheme for single-phase case

The proposed SVD-based MOR method considers an initial *n*th order rational approximation f_{VF}, obtained via VF, of a frequency-dependent function $f(s)$ for the frequency range Ω. The approximation f_{VF} can be expressed for the single-phase case as

$$f_{\mathrm{VF}} = \sum_{k=1}^{n} \frac{c_k}{s - p_k} + d. \tag{3.1}$$

Removing the contribution of the constant term *d*, (3.1) can be written as

$$h = f_{\mathrm{VF}} - d = \sum_{k=1}^{n} \frac{c_k}{s - p_k}. \tag{3.2}$$

Evaluation of (3.2) for the frequency range Ω with *N* frequency samples gives

$$h = Mx, \tag{3.3}$$

where

$$M = \begin{bmatrix} \frac{1}{s_1 - p_1} & \frac{1}{s_1 - p_2} & \cdots & \frac{1}{s_1 - p_n} \\ \frac{1}{s_2 - p_1} & \frac{1}{s_2 - p_2} & \cdots & \frac{1}{s_2 - p_n} \\ \vdots & \vdots & & \vdots \\ \frac{1}{s_N - p_1} & \frac{1}{s_N - p_2} & \cdots & \frac{1}{s_N - p_n} \end{bmatrix}, \tag{3.4}$$

$$x = \begin{bmatrix} c_1, & c_2, & \cdots, & c_n \end{bmatrix}^T \tag{3.5}$$

Note that complex poles and residues come in conjugate pairs (conjugate denoted by *), i.e., for two consecutive complex partial fractions k and k+1:

$$p_k = p_{k+1}^*, \quad c_k = c_{k+1}^*, \tag{3.6}$$

where:

$$p_k = p_k + jp_k, \quad c_k = c_k + jc_k. \tag{3.7}$$

To preserve the conjugacy, vector x in (3.5) is separated into real and imaginary parts, as indicated in (3.8). Matrix M is rearranged into a matrix M' with $M'_{l,k}$ and $M'_{l,k+1}$ representing the (l, k) and (l, k+1) elements of M', respectively, as shown in (3.9).

$$x^R = \left[c_1^r, \quad c_1^i, \quad c_3^r, \quad c_3^i, \quad \cdots, \quad c_{n-1}^r, \quad c_{n-1}^i \right]^T \tag{3.8}$$

$$M'_{l,k} = \frac{1}{s_l - p_k} + \frac{1}{s_l - p_k^*}, \quad M'_{l,k+1} = \frac{j}{s_l - p_k} - \frac{j}{s_l - p_k^*}, \quad l = 1,2,\cdots,N, \quad k = 1,2,\cdots,n. \tag{3.9}$$

Next, matrix M' is separated into its real and imaginary parts, resulting in

$$H = M^R x^R \tag{3.10}$$

where:

$$H = \begin{bmatrix} \mathrm{Re}\{h\} \\ \mathrm{Im}\{h\} \end{bmatrix}, \tag{3.11}$$

$$M^R = \begin{bmatrix} \mathrm{Re}\{M'\} \\ \mathrm{Im}\{M'\} \end{bmatrix}. \tag{3.12}$$

To simplify notation, M and x will be used hereafter instead of M^R and x^R respectively. To account for a partial frequency bandwidth, either low-frequency (LF) or high-frequency (HF), a diagonal weighting matrix W, with major effect on the specific frequency range, is applied to (3.10), resulting in

$$v = WH = WMx. \tag{3.13}$$

SVD is applied to the product WM of (3.13), yielding

$$v = U\Sigma V^T x. \tag{3.14}$$

Alternatively, system (3.14) can be expressed as

$$\Sigma V^T x = g, \tag{3.15}$$

where:

$$g = U^T v. \tag{3.16}$$

The singular values in Σ represent dynamics of the weighted matrix M. In this thesis, the Matlab® software [15] has been used to calculate the SVD decomposition providing Σ as diagonal matrix with the magnitude of the singular values ordered decreasingly. Then, the system (3.15) is truncated by selecting the r most significant singular values of the diagonal matrix Σ, with $r < n$, and taking the corresponding r rows of V^T; this results in

$$\Sigma_r V_r^T x = g_r \tag{3.17}$$

The solution vector x of (3.17) is obtained by using the Matlab® backslash operator '\' [15]. This results in a sparse vector x where the nonzero positions indicate the r partial fractions that are extracted from (3.2) to form the reduced-order system for the partial frequency bandwidth.

After application of SVD, as described above, the following reduced-order system is obtained:

$$h_r = \sum_{k=1}^{r} \frac{c_k}{s - p_k}. \tag{3.18}$$

Note that the poles of (3.18) are a subset of the original (stable) poles given by VF, thus keeping stability properties. The accuracy of the obtained reduced-order system is bounded by the initial approximation error by VF.

3.2 Solution scheme for multiphase case

In the multiphase case, we assume a frequency-dependent matrix function $F(s)$ of dimensions $m \times m$, and its corresponding matrix approximation of order n, provided by VF and assuming a common set of poles, given by [13,16]:

$$F(s)=\sum_{k=1}^{n}\frac{C_k}{s-p_k}+D, \tag{3.19}$$

where C_k represents an $m \times m$ residue matrix corresponding to pole k.

Removing the contribution of the constant term D in (3.19), results in

$$Q=F-D=\sum_{k=1}^{n}\frac{C_k}{s-p_k}. \tag{3.20}$$

To apply the SVD-based truncation to the multiphase case requires an especial matrix arrangement, as described next.

The direct transmission matrix D is arranged in row format, yielding

$$D=[d_{11},\ d_{12},\ \cdots,\ d_{1m},\ d_{21},\ d_{22},\ \cdots,\ d_{2m},\ \cdots,\ d_{m1},\ d_{m2},\ \cdots,\ d_{mm}], \tag{3.21}$$

where $d_{i,j}$ represents the (i^{th}, j^{th}) element of the D matrix. As for matrix F,

$$F=[f_{11}\ \ f_{12}\ \ \cdots\ \ f_{1m}\ \ f_{21}\ \ f_{22}\ \ \cdots\ \ f_{2m}\ \ \cdots\ \ f_{m1}\ \ f_{m2}\ \ \cdots\ \ f_{mm}], \tag{3.22}$$

Expression (3.22) shows that the elements of matrix function $F(s)$ have been arranged in column format for the N frequency samples, i.e., $f_{i,j}$ denotes the (i^{th}, j^{th}) element of the F matrix function evaluated for N frequencies and arranged as column. The resulting dimensions of D and F are $(m\times m)\times 1$ and $(m\times m)\times N$, respectively.

A typical column evaluation in (3.22), based on (3.20), for a single frequency point yields

$$f_{i,j} - d_{i,j} = \sum_{k=1}^{n} \frac{c_{i,j,k}}{s - p_k}, \qquad i = j = 1, 2, \cdots, m, \tag{3.23}$$

Note that evaluation of (3.23) implies the use of the set of poles only once, instead of m times. This evaluation also implies that residue matrix C of (2.14c) be arranged as

$$C = \begin{bmatrix} c_{1,1,1} & c_{1,2,1} & \cdots & c_{1,m,1} & c_{2,1,1} & c_{2,2,1} & \cdots & c_{2,m,1} & \cdots & c_{m,1,1} & c_{m,2,1} & \cdots & c_{m,m,1} \\ c_{1,1,2} & c_{1,2,2} & \cdots & c_{1,m,2} & c_{2,1,2} & c_{2,2,2} & \cdots & c_{2,m,2} & \cdots & c_{m,1,2} & c_{m,2,2} & \cdots & c_{m,m,1} \\ \vdots & \vdots & & \vdots & \vdots & \vdots & & \vdots & & \vdots & \vdots & & \vdots \\ c_{1,1,n} & c_{1,2,n} & \cdots & c_{1,m,n} & c_{2,1,n} & c_{2,2,n} & \cdots & c_{2,m,n} & \cdots & c_{m,1,n} & c_{m,2,n} & \cdots & c_{m,m,n} \end{bmatrix}, \tag{3.24}$$

resulting in dimensions of $n \times (m \times m)$.

Based on (3.21) to (3.24), evaluation of (3.20) for N frequency samples in a given frequency range Ω, provides the system

$$Q = Mx, \tag{3.25}$$

where $M \in \mathbb{C}^{N \times n}$ and $Q \in \mathbb{C}^{N \times (m \times m)}$

It is mentioned that matrix M in (3.25) has the same structure as in the single-phase case. Finally, (3.25) is separated into real and imaginary parts, weighted, and truncated via SVD, similarly to the single-phase case.

It is mentioned that alternative rational approximation techniques, such as Bode-based method, can be used within the proposed SVD-based MOR method.

3.3 Conclusions

The SVD-based MOR method applied to a specific frequency bandwidth for the single- and multiphase cases has been presented. The presented SVD-based method can be applied to a function (or matrix) when a specific frequency bandwidth phenomenon is under interest, e.g., overvoltages, switching, lightning, etc.

4 SVD-BASED MOR TECHNIQUE AND TIME-DOMAIN RESPONSE

In Chapter 3, the SVD technique is applied to a rational approximation in a specific frequency bandwidth to obtain a reduced-order system, amenable to EMT simulation. This Chapter describes the application of SVD to a rational approximation by partitioning a wide frequency range in two regions.

4.1 General steps

The complete time-domain response of the SVD-based MOR system can be achieved by following the next steps, where two small sets of poles are used for illustration purposes.

Step 1. A low-frequency approximation, f_{LF}, for range Ω_{LF} is obtained by applying the SVD-based MOR method to the original approximation given by VF, $f(s)$, as described in Chapter 3 and as illustrated in Fig. 4.1. It is assumed that the f_{LF} approximation involves the following sets of poles and residues, respectively:

$$p_{\mathrm{LF}} = \{a_1, \quad a_2, \quad a_3\}, \qquad\qquad c_{\mathrm{LF}} = \{c_1, \quad c_2, \quad c_3\} \tag{4.1}$$

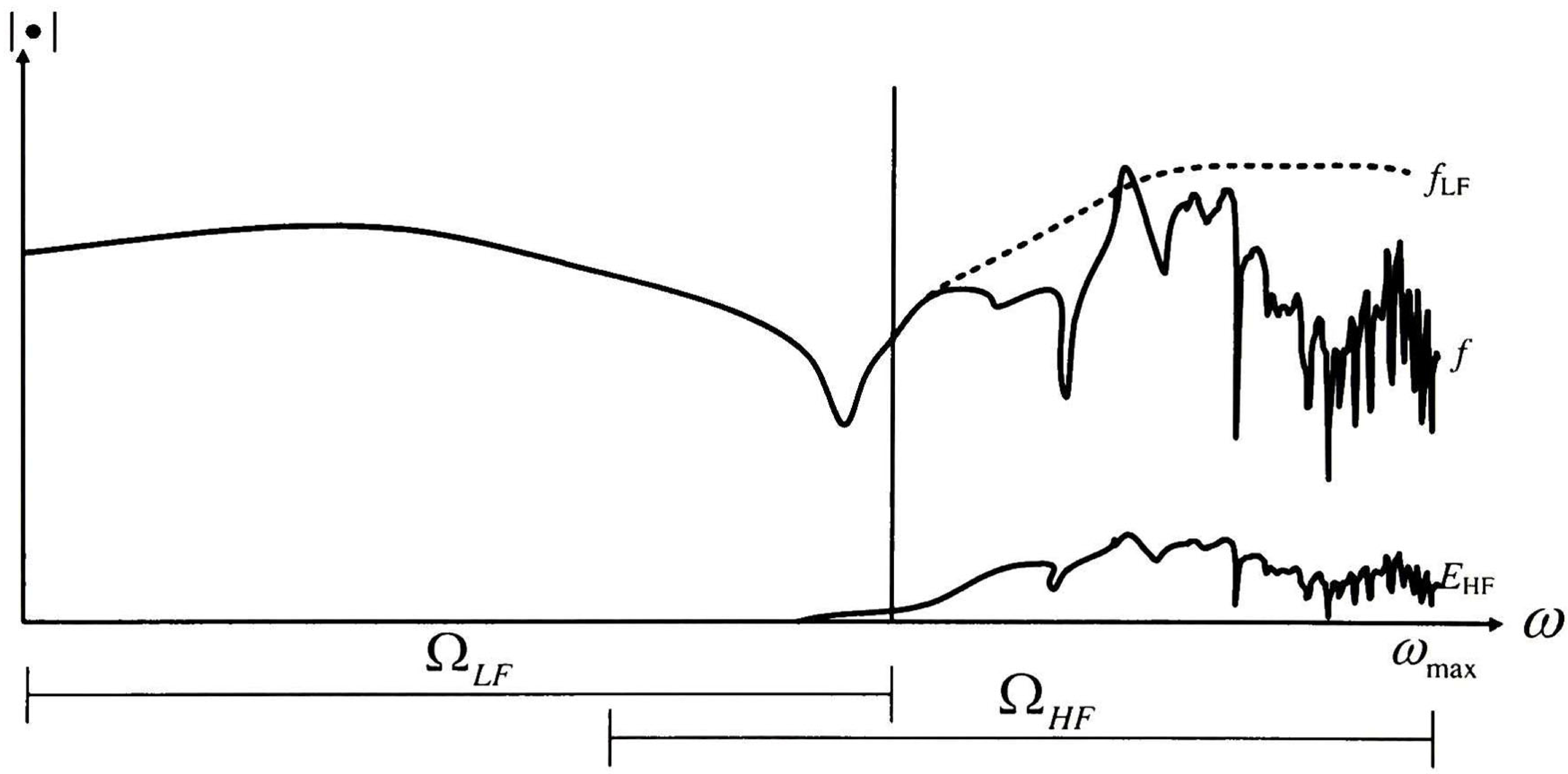

Fig. 4.1. Illustration of f_{LF} approximation and E_{HF} error

Step 2. The error (E_{HF}) between the $f(s)$ and f_{LF} approximations, evaluated in range Ω_{HF}, is calculated and approximated via rational functions, see Fig. 4.1. This is justified a) by the assumption of obtaining a good LF approximation of $f(s)$ and b) to obtain an appropriate interfacing of poles and zeros from LF to HF.

Step 3. The SVD-based MOR method is applied to E_{HF} from step 2 obtaining the following sets of poles and residues:

$$p_{E_{\mathrm{HF}}} = \{a_2,\ a_3,\ a_4,\ a_5\}, \qquad c_{E_{\mathrm{HF}}} = \{c_2',\ c_3',\ c_4,\ c_5\}. \tag{4.2}$$

Note that f_{LF} and E_{HF} approximations share some poles, i.e., a_2 and a_3.

Step 4. The unshared poles from p_{LF} are included into $p_{E_{\mathrm{HF}}}$, thus forming a new single set of poles. This yields approximation $f_{\mathrm{LF+HF}}$, having the following sets of poles and residues:

$$\begin{aligned} p_{\mathrm{LF+HF}} &= \{a_1,\ a_2,\ a_3,\ a_4,\ a_5\}, \\ c_{\mathrm{LF+HF}} &= \{c_1,\ c_2'',\ c_3'',\ c_4,\ c_5\}, \end{aligned} \tag{4.3}$$

where:

$$c_2'' = c_2' + c_2, \qquad c_3'' = c_3' + c_3. \tag{4.4}$$

Note that, in (4.3), the shared poles are not repeated and its corresponding residues are added up.

Step 5. The fast dynamics ranging from t_o to t_{sw} (sw denotes switching time) are calculated by using the $f_{\mathrm{LF+HF}}$ approximation, Fig. 4.3.

Step 6. The time-domain response from t_{sw} to t_f is calculated by using the f_{LF} approximation, Fig. 4.3.

Based on steps 5 and 6, the time-domain response is simulated using $f_{\mathrm{LF+}HF}$ first, then a set of initial conditions have to be obtained for the starting simulation of f_{LF} at $t = t_{sw}$. Computation of initial conditions is presented section 4.3. Also, it is noted that the $f_{\mathrm{LF+HF}}$ approximation involves more poles than the E_{HF} approximation; however, the $f_{\mathrm{LF+HF}}$ approximation is only used while the fast dynamics last. Several experiments show that few poles, e.g., one to five, are unshared; thus, the dimensions of $f_{\mathrm{LF+HF}}$ are not substantially increased compared to $f_{E_{HF}}$. An interesting feature of the procedure above is that the simulation of f_{LF} can utilize a time-step larger than the one used for f_{LF+HF} simulation. A flowchart of the outlined procedure is presented in Fig. 4.2.

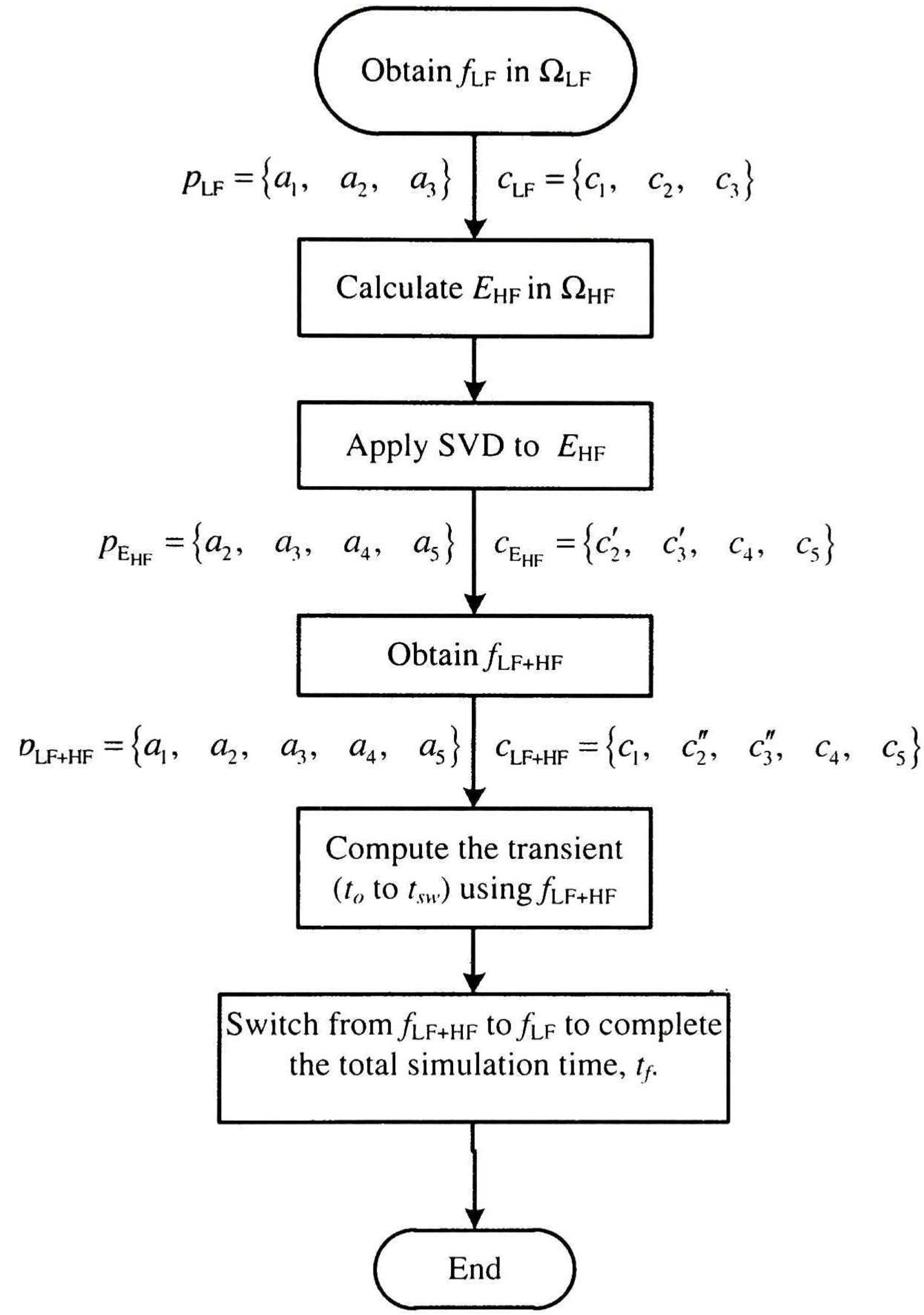

Fig. 4.2. Flowchart of general steps

4.2 Discretization of ODEs

Due to f_{LF+HF} and f_{LF} are obtained from an original rational approximation given by VF, they can be expressed as linear time-invariant (LTI) systems in the state-space domain, generically represented by

$$\begin{aligned} \dot{x} &= Ax + Bu \\ y &= Cx + du \end{aligned} \tag{4.5}$$

The trapezoidal rule of integration applied to (4.5) results in [17]:

$$x_{k+1} = x_k + \frac{\Delta t}{2}\left[A\left(x_k + x_{k+1}\right) + B\left(u_k + u_{k+1}\right)\right]. \tag{4.6}$$

where time has been discretized as $t = t_o, t_1, \ldots, t_f$,with $t_k = k\Delta t$.

Rearranging (4.6), results in

$$\left(\mathrm{I} - \frac{\Delta t}{2}A\right)x_{k+1} = \left(\mathrm{I} + \frac{\Delta t}{2}A\right)x_{k+1} + \frac{\Delta t}{2}B\left(u_k + u_{k+1}\right), \tag{4.7}$$

where I represents an identity matrix of appropriate dimensions.

Equation (4.7) can be expressed in compact form as

$$Lx_{k+1} = Mx_k + B_d u_{av}, \tag{4.8}$$

where

$$L = \mathrm{I} - \frac{\Delta t}{2}A, \quad M = \mathrm{I} + \frac{\Delta t}{2}A, \quad B_d = \Delta t B, \quad u_{av} = \frac{u_k + u_{k+1}}{2}$$

From (4.8), x_{k+1} is obtained as

$$x_{k+1} = L^{-1}\left(Mx_k + B_d u_{av}\right), \tag{4.9}$$

From (4.5) the time-domain output is given by

$$y_{k+1} = Cx_{k+1} + du_{k+1}, \tag{4.10}$$

The time-domain simulation starts with the approximation f_{LF+HF} expressed as the state-space system (4.5) and discretized as in (4.9)-(4.10), and runs until a predetermined simulation time t_{sw}, Fig. 4.3.

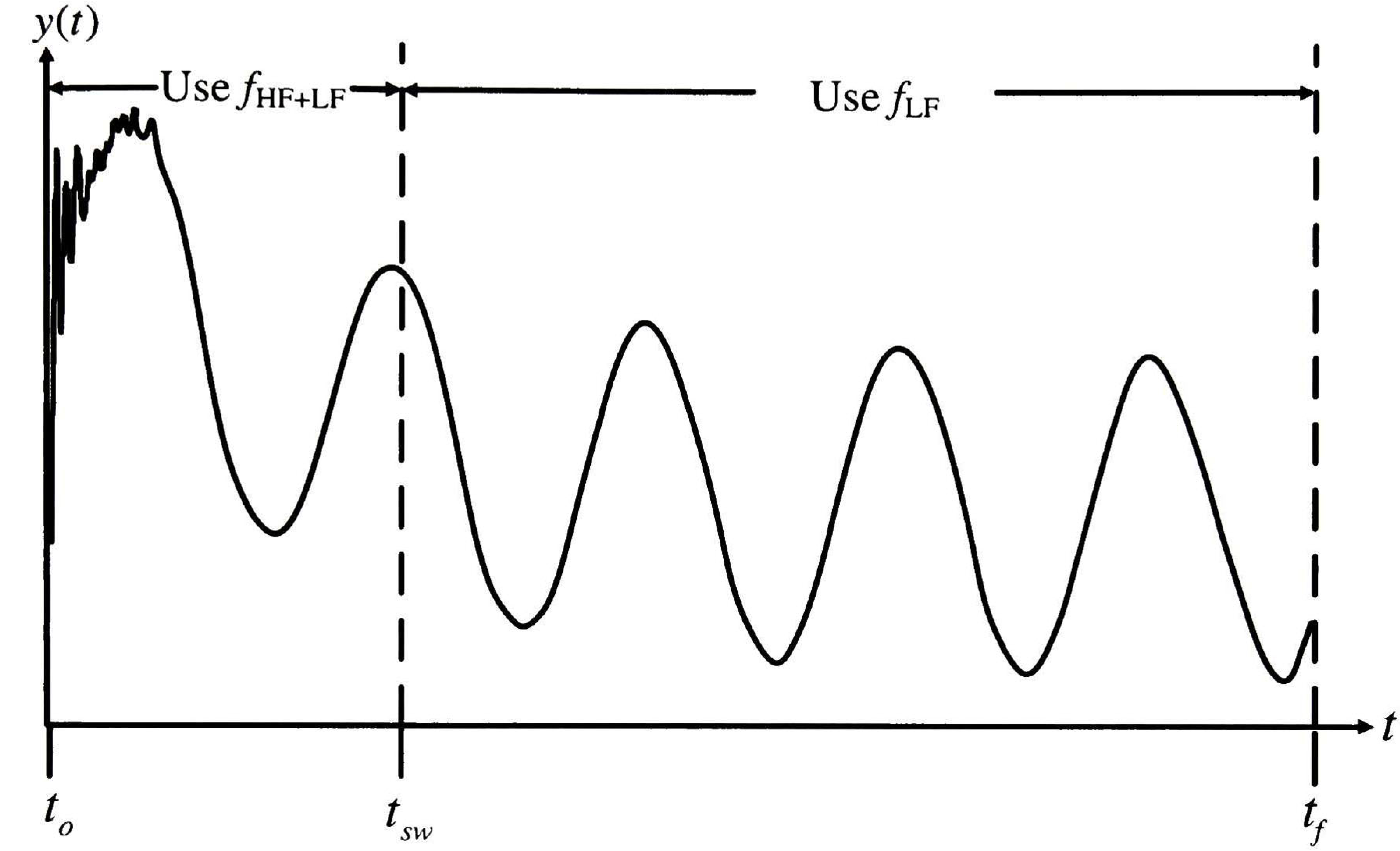

Fig. 4.3 System configuration of time-domain simulation of f_{LF+HF} and f_{LF} approximations

4.3 Computation of initial conditions

The change from simulating the response of the f_{LF+HF} system to the simulation of f_{LF} at time $t = t_{sw}$ (corresponding to time-step k+1) is achieved by using an appropriate set of initial conditions for the f_{LF} approximation.

To obtain the appropriate set of initial conditions for f_{LF}, consider the numerical solution of the f_{LF+HF} system at time t_{sw}, represented as the state vector x_{k+1}^{LF+HF} and its corresponding output y_{k+1}^{LF+HF} as given by (4.11). For illustration purposes, only five states are included in (4.11).

$$x_{k+1}^{\mathrm{LF+HF}} = \begin{bmatrix} x_1^{\mathrm{LF+HF}} \\ x_2^{\mathrm{LF+HF}} \\ x_3^{\mathrm{LF+HF}} \\ x_4^{\mathrm{LF+HF}} \\ x_5^{\mathrm{LF+HF}} \end{bmatrix}_{k+1} \qquad y_{k+1}^{\mathrm{LF+HF}} = c_{\mathrm{LF+HF}} x_{k+1}^{\mathrm{LF+HF}} + du_{k+1}, \tag{4.11}$$

In addition, the state vector and the output for the f_{LF} approximation at t_{sw} are expressed as:

$$x_{k+1}^{\mathrm{LF}} = \begin{bmatrix} x_1^{\mathrm{LF}} \\ x_2^{\mathrm{LF}} \\ x_3^{\mathrm{LF}} \end{bmatrix}_{k+1} \qquad y_{k+1}^{\mathrm{LF}} = c_{\mathrm{LF}} x_{k+1}^{\mathrm{LF}} + du_{k+1}, \tag{4.12}$$

where, for illustration purposes, only three states are assumed. Note that the constant term d in (4.11) and (4.12) is the same due to its effect has been removed in (3.2).

At $t = t_{sw}$, output $y_{k+1}^{\mathrm{LF+HF}}$ equals the output of the f_{LF} system y_{k+1}^{LF}, noting that p_{LF} represents a subset of $p_{\mathrm{LF+HF}}$. Then, based on (4.4) and (4.10), the initial condition state vector for f_{LF} is given by x_{k+1}^{LF} which is obtained as a subset of $x_{k+1}^{\mathrm{LF+HF}}$; this is represented by

$$\begin{bmatrix} x_1^{\mathrm{LF}} \\ x_2^{\mathrm{LF}} \\ x_3^{\mathrm{LF}} \end{bmatrix}_{k+1} = \begin{bmatrix} x_1^{\mathrm{LF+HF}} \\ x_2^{\mathrm{LF+HF}} \\ x_3^{\mathrm{LF+HF}} \end{bmatrix}_{k+1} \tag{4.13}$$

This direct transition is due to the assumption of having fitted the error function E_{HF}, yielding a direct relation between elements of subsets c_{LF} and $c_{\mathrm{LF+HF}}$, as shown in (4.4). Thus, the time-domain response is carried on using the f_{LF} approximation with x_{k+1}^{LF} from (4.13) as initial conditions at t_{sw}.

4.4 Computation of rms error

The *rms* error of the time-domain output given by the SVD-based MOR method, taking as reference the full-size system initially obtained by VF, is calculated in this thesis with:

$$e_{rms} = \sqrt{\frac{\int (y_{\mathrm{VF}} - y_{\mathrm{SVD}})^2 dt}{\int {y_{\mathrm{VF}}}^2 dt}}, \tag{4.14}$$

where y_{VF} corresponds to the time-domain response achieved with VF and y_{SVD} is the output obtained by using the SVD-based MOR method.

4.5 Conclusions

In this Chapter, the general MOR methodology based on SVD has been presented. It has been shown that a direct transition between the simulation of LF and HF reduced-order approximations is achieved by fitting the function error between the original function and the f_{LF} function.

5 CASE STUDIES

In this Chapter, the SVD-based MOR method, described in Chapters 3 and 4, is validated by using two illustrative examples (single- and three-phase systems). Also, its accuracy and computational features are shown. All time-domain responses, CPU times, and errors obtained with the proposed method are compared with the original full-order approximation computed by VF. All the results presented in this Chapter have been obtained using 1000 frequency samples. An Intel® Core 2 Duo, CPU E6750 @ 2.66 GHz, 2 GB RAM computer has been utilized.

5.1 Case study 1: single-phase network

5.1.1 Network description

As first example, the single-phase network presented in Fig. 5.1 is adopted. The network consists of seven identical single-phase overhead transmission lines and two underground cables (UC) buried at 1m which have the same geometry, Fig. 5.2. All the parameters of the overhead lines, underground cables, loads, source, and input impedance are given in Table 5.1

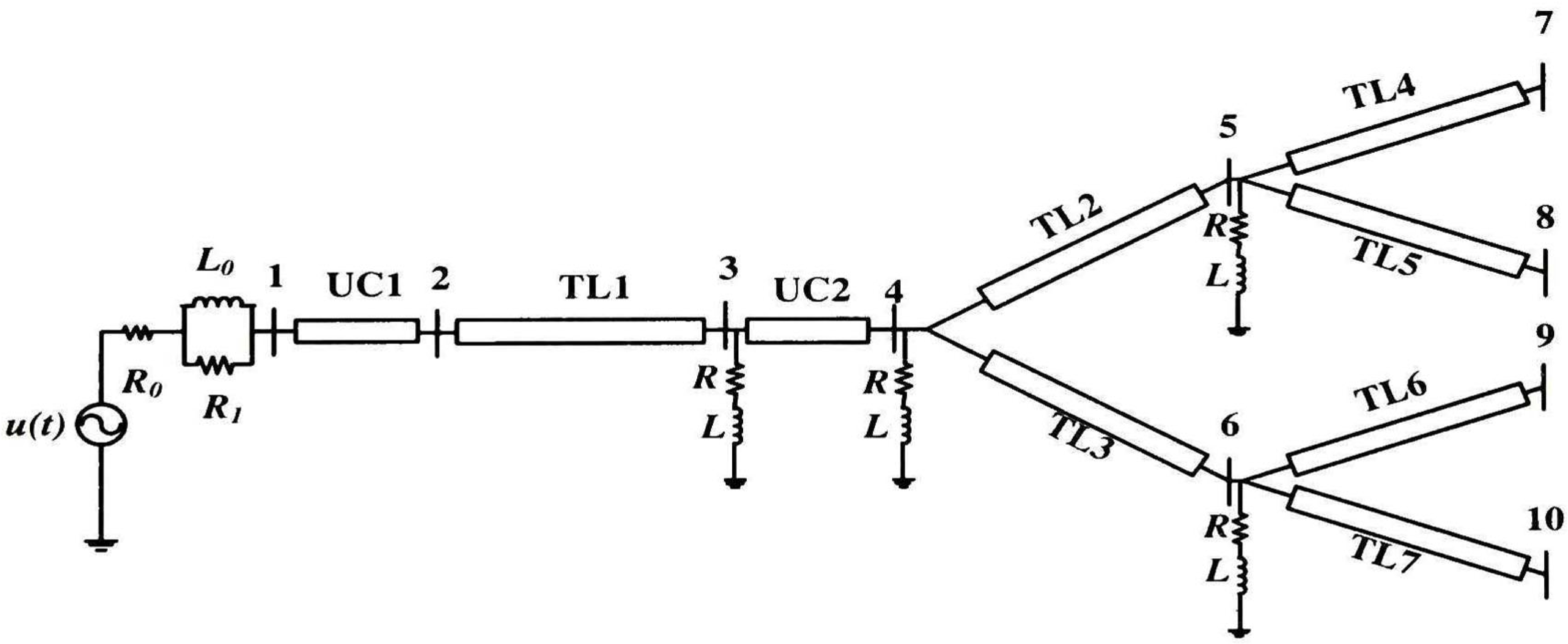

Fig. 5.1. Single-phase network for case study 1.

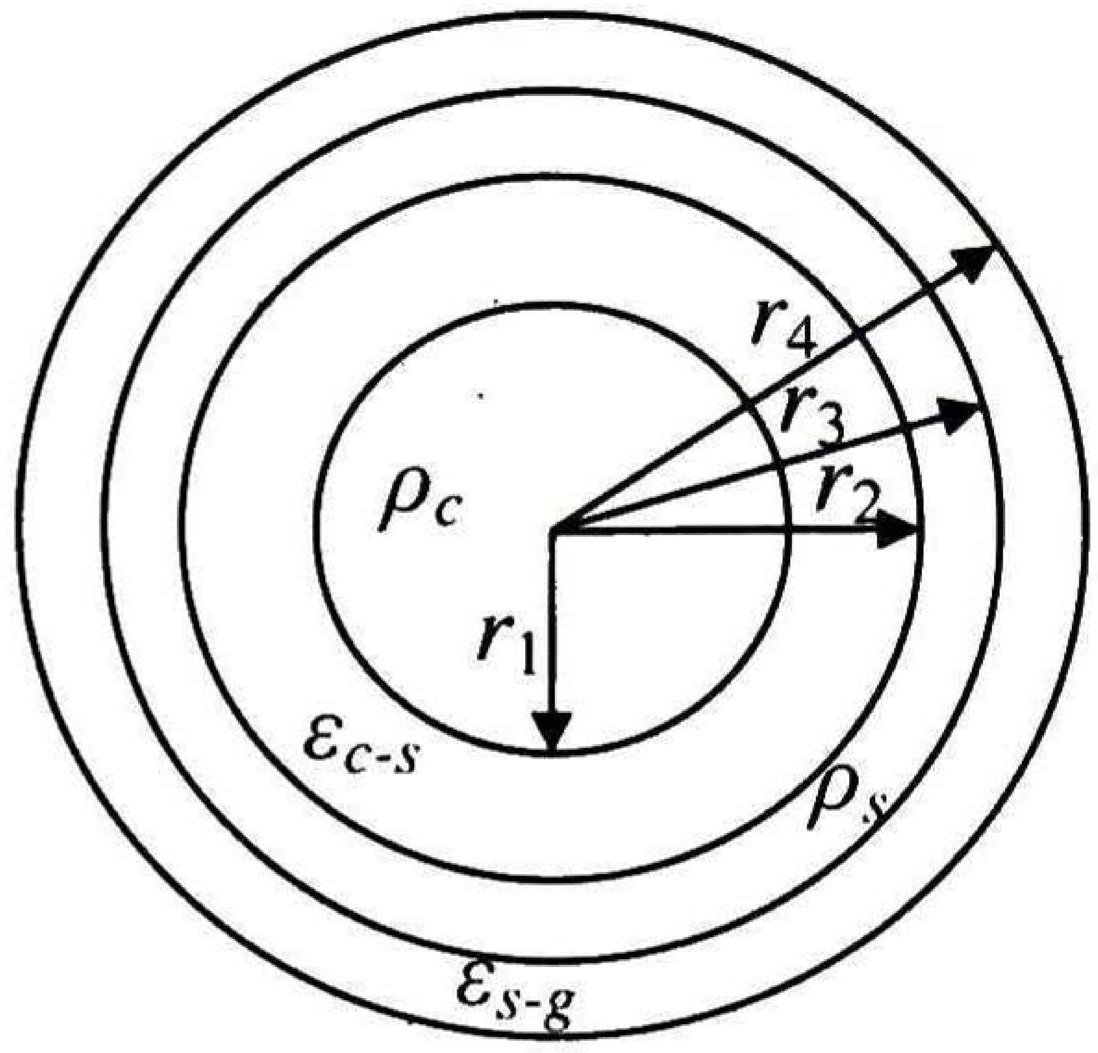

Fig. 5.2. Underground cable configuration.

Table 5.1. Network parameters, case study 1.

Symbol	Value	Description
	Overhead lines	
l_l	10 km	Length
h	15 m	Height
r_c	1 cm	Conductor radius
	8.9954×10^{-5} Ω /m	DC resistance
	Underground cables	
l_c	5 km	Length
r_1	1.95 cm	Radius 1
r_2	3.77 cm	Radius 2
r_3	3.79 cm	Radius 3
r_4	4.25 cm	Radius 4
ρ_c	3.365×10^{-8} Ω-m	Conductivity
$\varepsilon_{c\text{-}s}$	2.85	Relative permittivity
ρ_s	1.718×10^{-8} Ω-m	Conductivity
$\varepsilon_{s\text{-}g}$	2.51	Relative permittivity
	Loads	
R	100 Ω	Resistance
L	0.1 H	Inductance
	Source and Input Impedance	
R_o	0.01 Ω	Resistance
L_o	0.0002 H	Inductance
R_1	800 Ω	Resistance

5.1.2 Rational approximation by VF

The driving-point admittance seen from the left terminal of UC1 (bus 1) is calculated as shown in Appendix A and evaluated for the frequency range Ω = {10Hz, 1MHz}. The analytical evaluation of the driving-point admittance is presented in Fig. 5.3 as a continuous trace; the dashed trace in Fig. 5.3 shows the approximation obtained via VF for the complete frequency range Ω, using an order of n = 70 and an RMS error of 4.059×10^{-4} Due to the good accuracy of the VF approximation, the difference with the original driving-point admittance curve cannot be observed in Fig. 5.3.

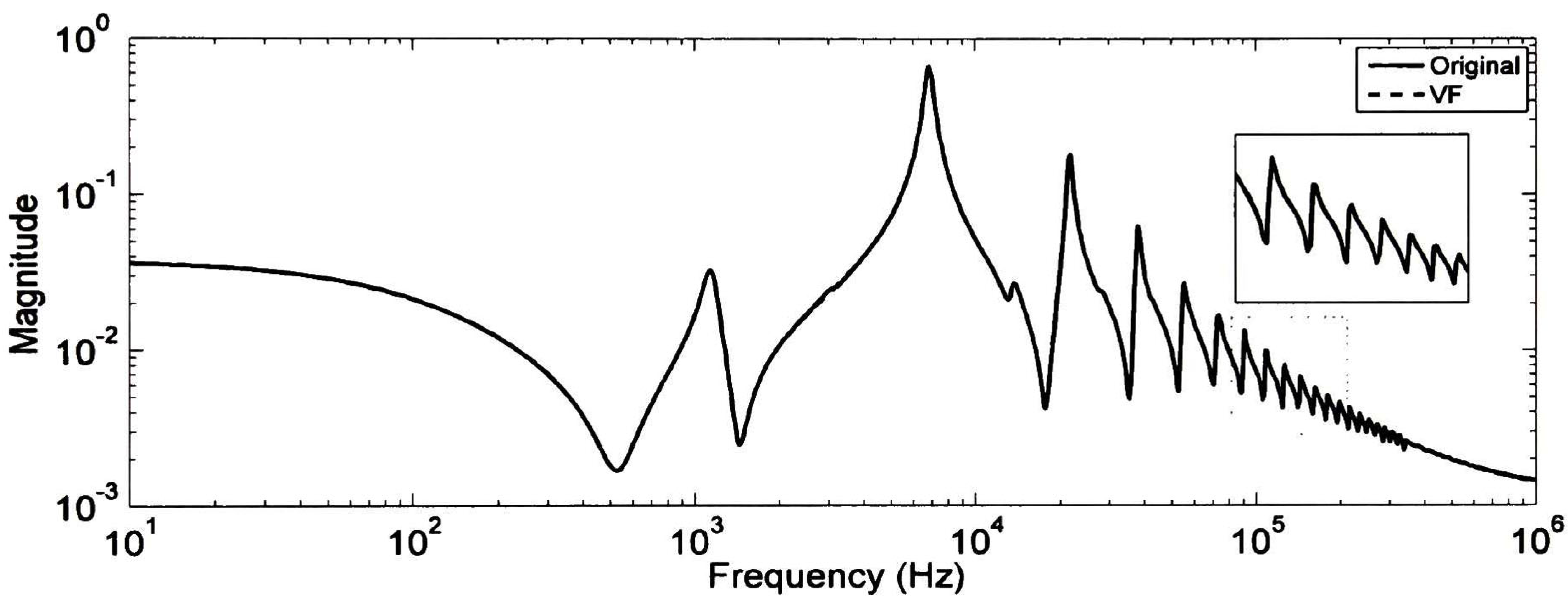

Fig. 5.3. Single-phase driving-point admittance and approximation obtained by VF.

5.1.3 SVD-based MOR method applied to Ω_{LF} and Ω_{HF} ranges

The proposed SVD-based MOR method is applied to both the approximated input-admittance and the error function E_{HF} in the frequency ranges: Ω_{LF} = {10 Hz, 10 kHz} and Ω_{HF} = {1 kHz, 1 MHz}, respectively. The singular values resulting from the application of the proposed technique in Ω_{LF} and Ω_{HF} are presented in Figs. 5.4(a) and 5.4(b), respectively. Based on the obtained singular values, orders of r_{LF} = 10 and r_{HF} = 37 are chosen for the rational approximations f_{LF} and E_{HF}, respectively. Singular value result of additional tests, are shown in Table 5.2. The resultant f_{LF} approximation with r_{LF} = 10 is presented in Fig. 5.5(a) as a dashed trace and compared with the approximation by VF.

As discussed in Chapter 3, the SVD-based MOR is expected to produce unshared poles between the f_{LF} approximation and the approximation of the error function E_{HF}. For this case study, only one unshared pole has been added to E_{HF}, and the new residues are computed as in (4.4), resulting in f_{LF+HF}. The obtained f_{LF+HF} approximation with $r_{LF+HF} = 38$ is shown in Fig. 5.5(b) and compared with the approximation by VF.

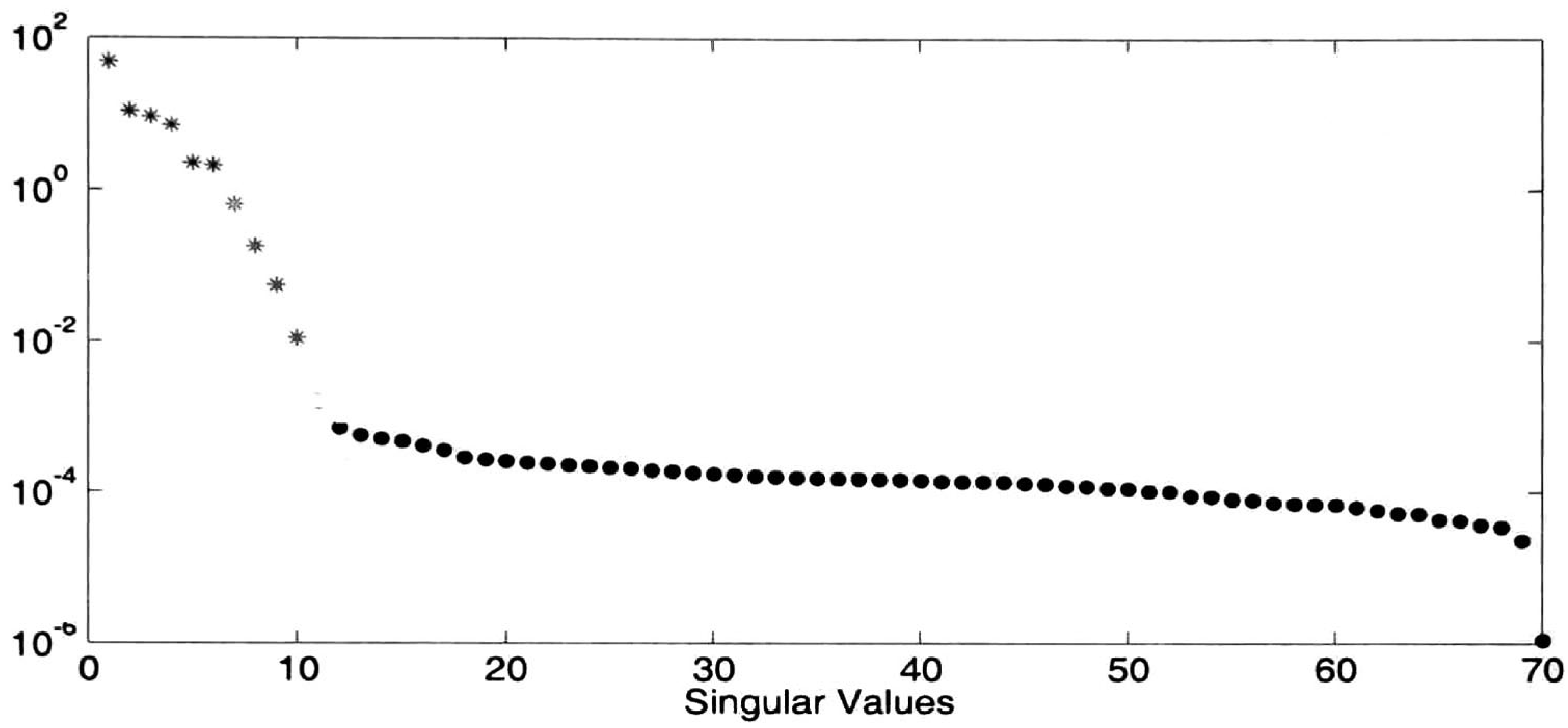

(a)

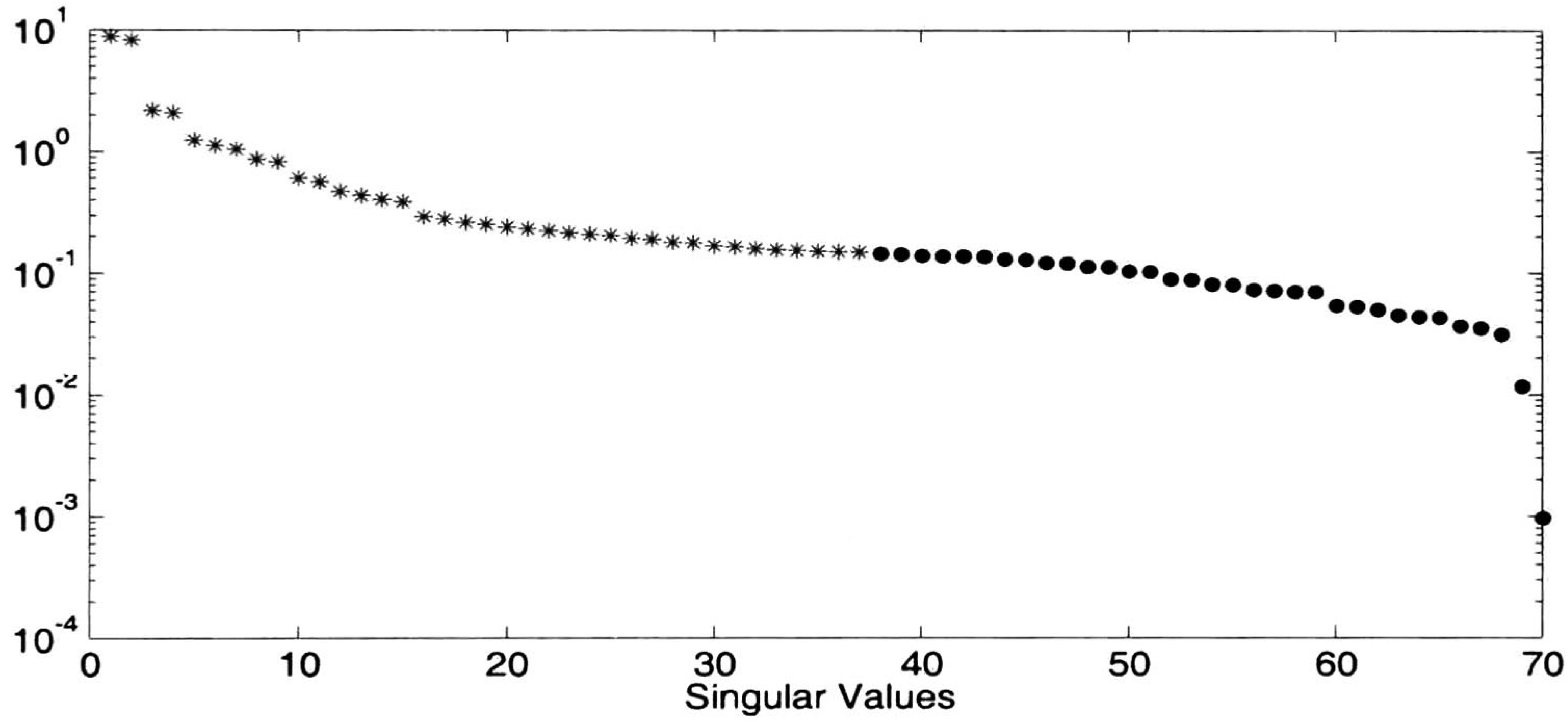

(b)

Fig. 5.4. Singular values obtained when applying SVD-based method (a) to rational approximation of Fig. 5.3 in range Ω_{LF} and (b) to E_{HF} in range Ω_{HF}

Table 5.2. Singular value ratios for E_{HF} and f_{LF} approximations.

r_{LF}	$\sigma_{r_{LF}}/\sigma_1$	r_{HF}	$\sigma_{r_{HF}}/\sigma_1$
8	3.712×10^{-3}	29	2.016×10^{-2}
10	2.273×10^{-4}	37	1.686×10^{-2}

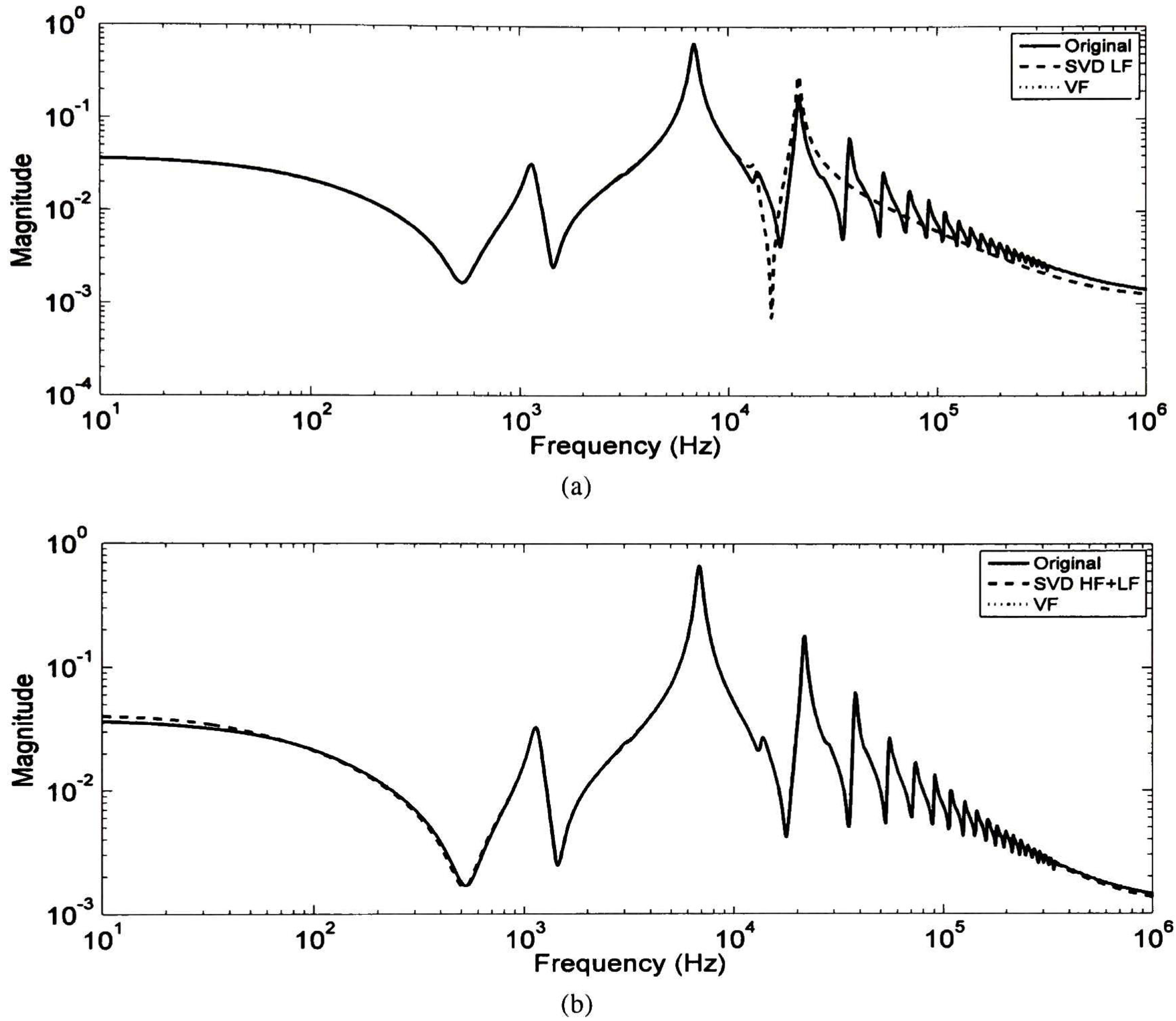

Fig. 5.5. Approximation of driving-point admittance using the SVD-based MOR method (a) f_{LF}, order 10, and (b) f_{LF+HF}, order 38.

5.1.4 Time-domain response

The network of Fig. 5.1 is employed to simulate a transient response. The time-domain response is obtained using an integration time-step of 1 μs for the full- and reduced-order approximations for the complete observation time of 30 ms. The time-domain input, applied at $t = 0$ s, is assumed as the following voltage source (with ω_0=377 rad/s):

$$u(t) = \sin(\omega_0 t) + 0.3\sin(3\omega_0 t + \pi/3) + 0.1\sin(5\omega_0 t) + 0.1\sin(7\omega_0 t) + 0.05\sin(15\omega_0 t) .$$

For this case study, the complete simulation time is divided in two time subwindows, i.e., a) $t_1 = \{0 \leq t \leq t_{sw}\}$ and b) $t_2 = \{t_{sw} < t \leq 0.03 \text{ s}\}$, with $t_{sw} = 6\times10^{-4}$ s. In a), the $f_{\text{LF+HF}}$ 38$^{\text{th}}$ order approximation is used, while in b), the f_{LF} 10$^{\text{th}}$ order approximation is employed. In contrast, the f_{VF} 70$^{\text{th}}$ order approximation by VF is simulated as the full-order system (taken as reference) for the complete observation time.

Fig. 5.6(a) shows the simulated transient currents obtained with both the full- and the SVD-based MOR systems for the complete observation time. Fig. 5.6(b) presents the first 0.5 ms noting that a good agreement between the two responses is observed.

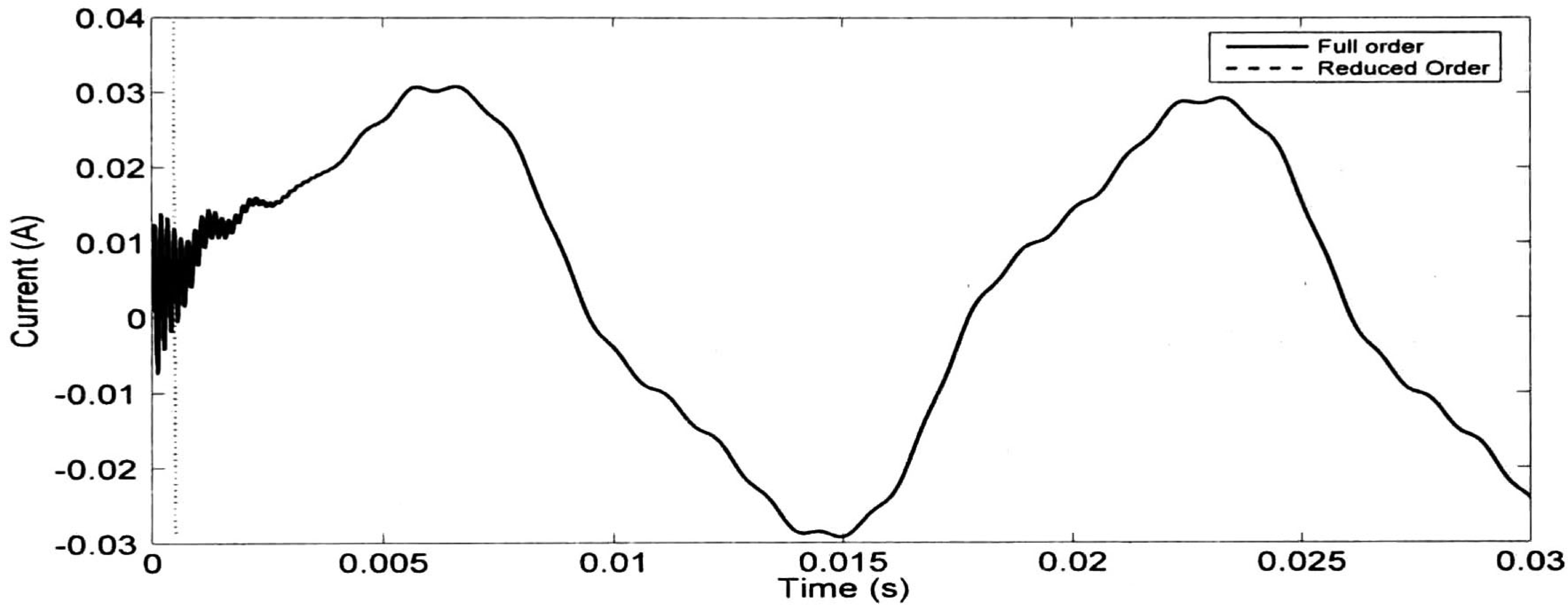

(a)

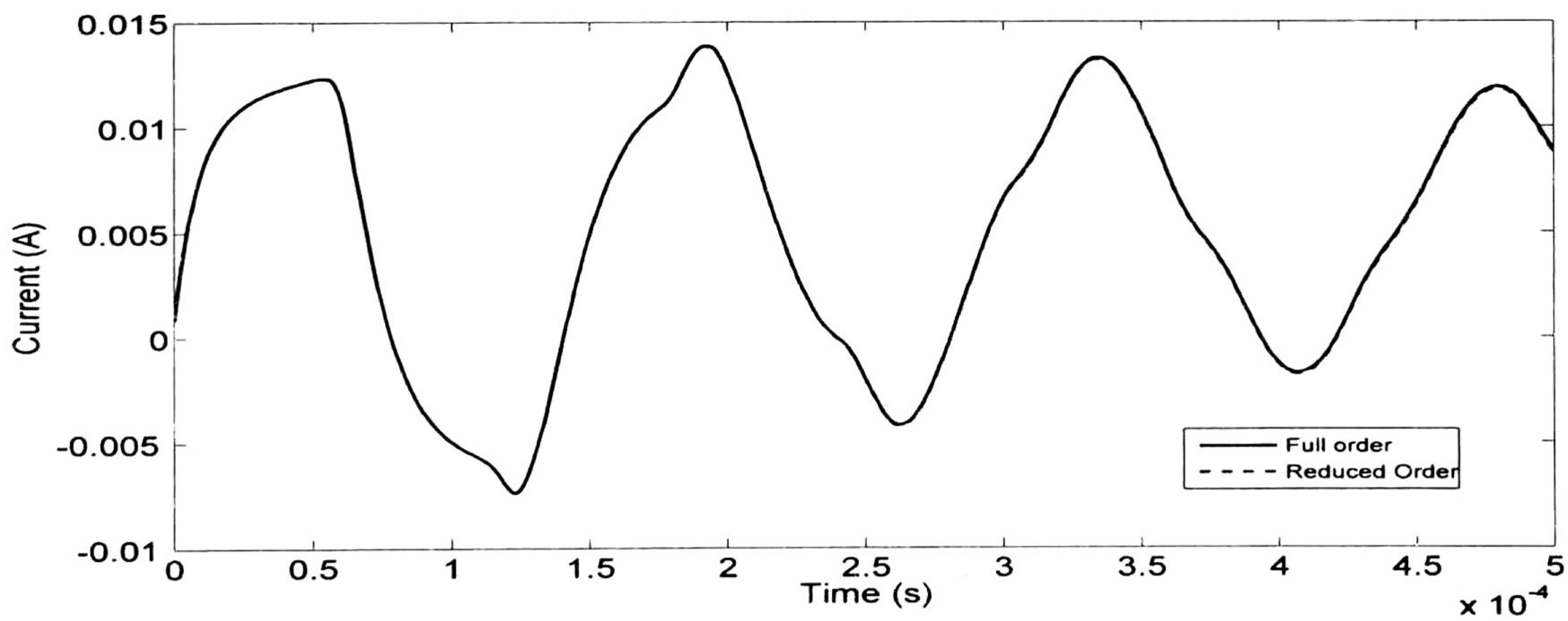

(b)

Fig. 5.6. (a) Transient waveforms by the full-order approximation given by VF and by the SVD-based MOR method, (b) close up.

Table 5.3 presents further experimental results using several reduction orders of f_{LF} and E_{HF}. The results in Table 5.3 have been obtained assuming fixed LF and HF ranges. Also, in Table 5.3 r_{LF}, $r_{E_{HF}}$, and r_{LF+HF} correspond to orders for the f_{LF}, E_{HF}, and f_{LF+HF} approximations, respectively.

The *rms* errors and CPU times obtained by using the full-order approximation given by VF and the reduced-order system by the proposed SVD-based method are also shown in Table 5.3. Table 5.3 shows that the *rms* error given by the proposed method is less than 1% for all cases. Table 5.3 also shows that the CPU time by the full-order simulation is about seven times larger than the required by the SVD-based MOR model.

To further validate the proposed SVD-based MOR method, the last two rows of Table 5.3 present the results obtained when applying the SVD-MOR and balanced realization (BR) methods to the complete frequency range. It can be observed that the full-order 70th approximation originally given by VF has been reduced to order 38 with good accuracy by both methods; however, the CPU times are not comparable to the one given by the proposed SVD-based MOR method. Note that the CPU time employed by the BR method is even longer than the CPU time required by the full-order approximation due to BR method yields full state matrix A corresponding to the reduced-order system, instead of a diagonal matrix A, thus impacting the CPU time. Also, it is noted that the order of the reduced system is the same along the simulation by the SVD and BR methods applied to the complete frequency range.

Table 5.3. RMS error in the output and CPU time for different SVD-based MOR approximations.

	r_{LF}	$r_{E_{HF}}$	r_{LF+HF}	e_{rms}	CPU Time (s)
VF	70				0.24989
SVD-based MOR	8	29	30	0.0035988	0.035013
	8	37	38	0.0032849	0.035214
	10	29	30	0.0017640	0.037957
	10	37	38	0.0016252	0.038328
SVD	38			0.0014021	0.134550
BR	38			3.87×10^{-5}	0.586100

An advantage of the proposed method is that further computational savings, without losing too much accuracy, can be achieved by using a larger time-step when simulating f_{LF} for $t > t_{sw}$. Table 5.4 shows the e_{rms} and CPU times when using 1 μs and 5 μs time-steps for the simulation of f_{LF+HF} and f_{LF}, respectively. Comparison of Tables 5.3 and 5.4 shows that the CPU time required when using different integration time-steps is about four times less than the employed when using a single time-step.

Table 5.4. RMS error in the output and CPU time for different SVD-based MOR approximations when using two different time integration steps.

	r_{LF}	r_{LF+HF}	Δt = 1μs/5μs	
			e_{rms}	CPU Time (s)
SVD-based MOR	8	30	0.0037119	0.0076016
	8	38	0.0033015	0.0080847
	10	30	0.0032125	0.0084115
	10	38	0.0030235	0.0087659

5.2 Case study 2: three-phase network

5.2.1 Network description

In this case study, we apply the SVD-based MOR to a modified version of the 66 kV three-phase network taken from [18] and depicted in Fig. 5.7. The network consists of ten overhead lines and one underground cable of 30 km long, which has been added to the original network and located next to the source. The overhead line lengths and load parameters are given in Tables 5.5 and 5.6.

Table 5.5. Overhead line lengths.

Name	Length (Km)	Name	Length (Km)
TL1	400	TL6	400
TL2	200	TL7	400
TL3	30	TL8	500
TL4	40	TL9	400
TL5	400	TL10	400

Table 5.6. Load parameters.

Name	Resistance (Ω)	Inductance (mH)	Name	Resistance (Ω)	Inductance (mH)
L1	350	50	L6	250	10
L2	250	50	L7	250	10
L3	350	50	L8	350	10
L4	250	50	L9	250	10
L5	250	50	L10	250	10

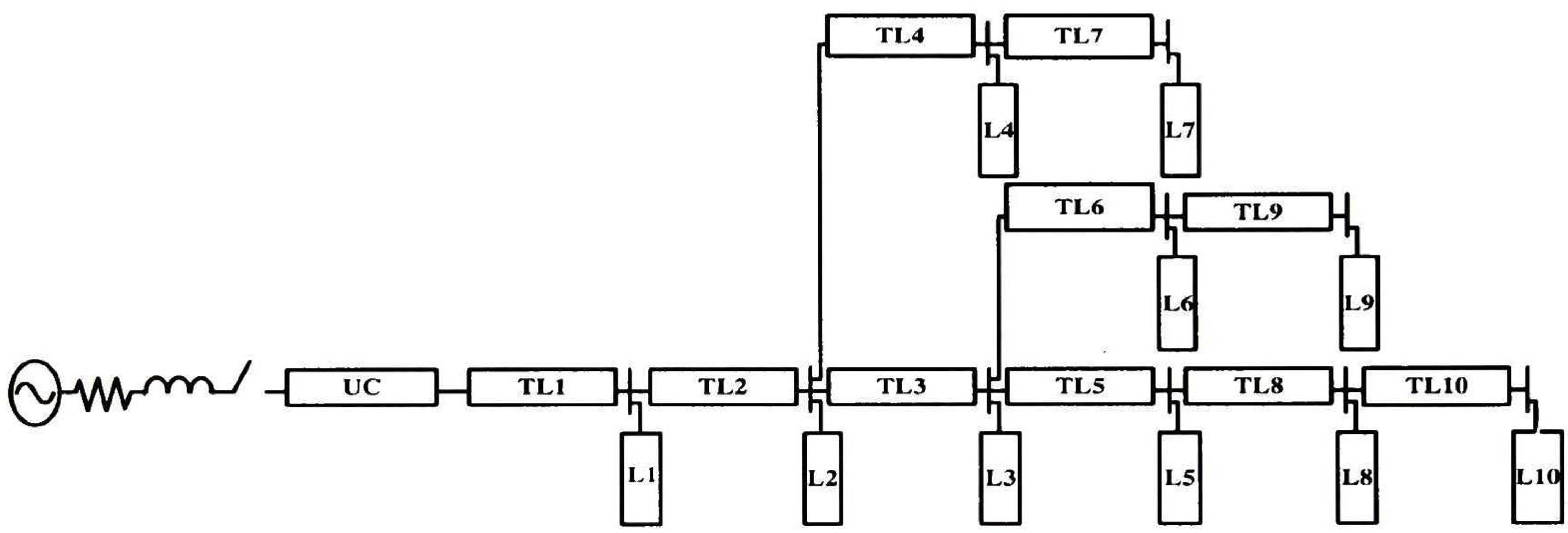

Fig. 5.7. Network configuration of three-phase network, case study 2 [18].

5.2.2 Rational approximation by VF and SVD-based MOR method applied to Ω_{LF} and Ω_{HF} ranges

For this case study, the driving-point admittance is calculated (see Appendix B for details) and fitted via VF within the complete frequency range assumed as Ω = {1 Hz to 5 kHz}. VF yields a passive full-order approximation of the driving-point admittance, shown in Fig. 5.8(a) with an RMS approximation error of 7.311×10^{-5} and order of 148. It is important to mention that the number of state variables for multiphase systems is different of the order approximation. For this case study, the number of state variables of the full-order approximation is 444. Next, the proposed SVD-based method is applied to the driving-point admittance and to the error function E_{HF} in the ranges: Ω_{LF} = {1 Hz to 1 kHz} and Ω_{HF} = {10 Hz to 5 kHz}, respectively. Based on the obtained singular values, orders of r_{LF} = 35 and r_{HF} = 118 are chosen for f_{LF} and E_{HF}, respectively. The corresponding singular value ratios are: σ_{35}/σ_1 = 6.488×10^{-6} and σ_{118}/σ_1 = 1.560×10^{-3}. Five unshared poles result from the comparison of the truncated systems f_{LF} and E_{HF}. Therefore, the f_{LF+HF} approximation results in an order of 123. The resultant f_{LF} and f_{LF+HF} approximations (both, as a dashed trace) are presented in Figs. 5.8(b) and 5.8(c), respectively, and compared with the original full-order approximations by VF (continuous trace).

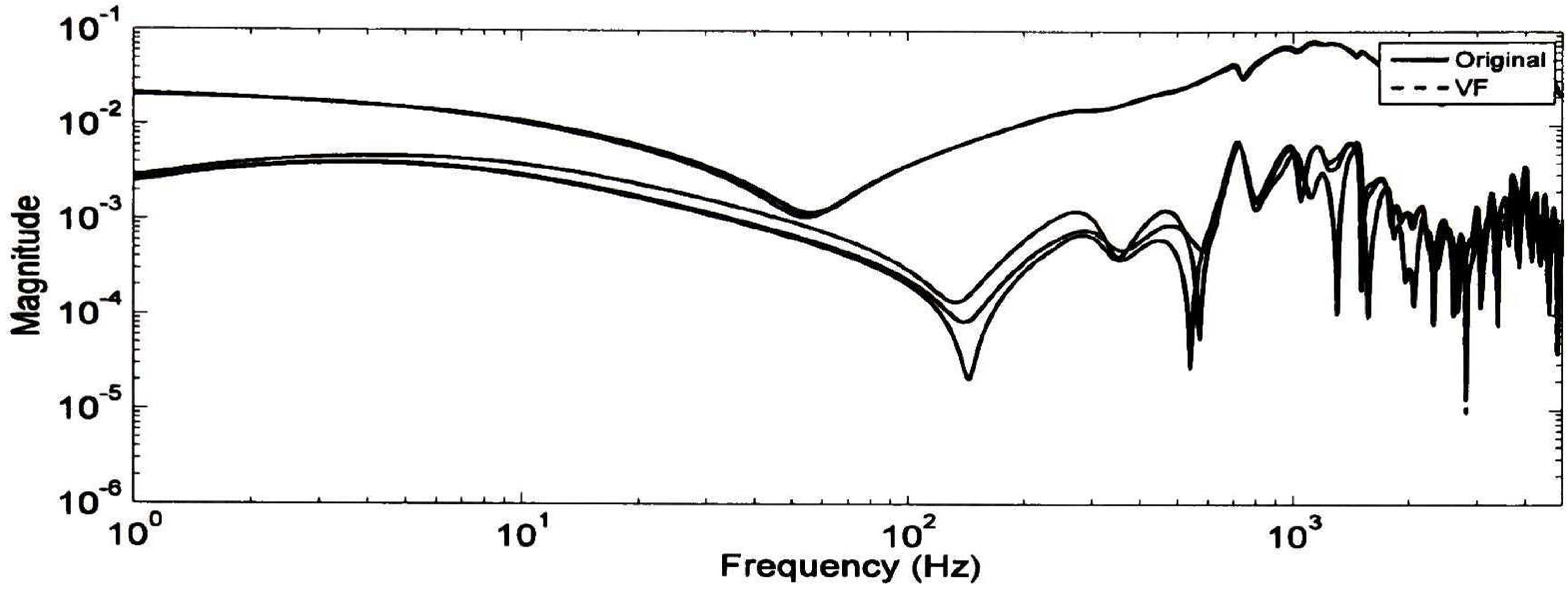

(a)

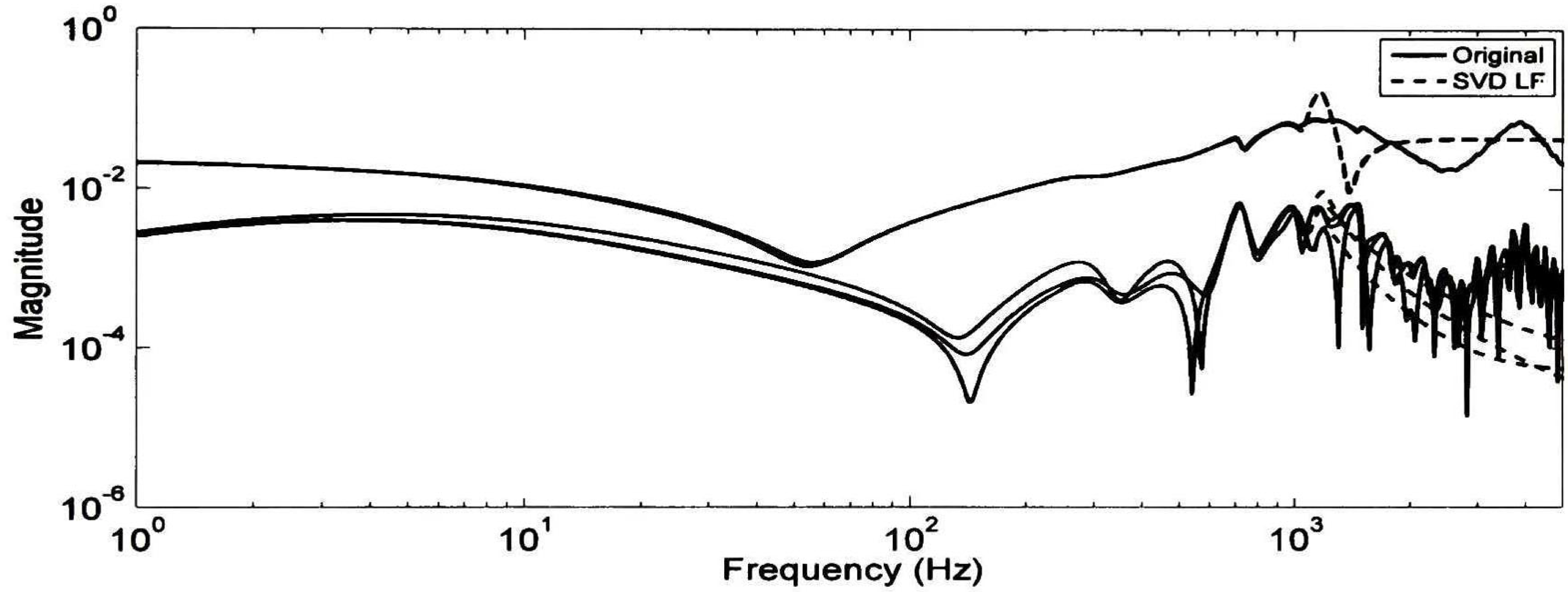

(b)

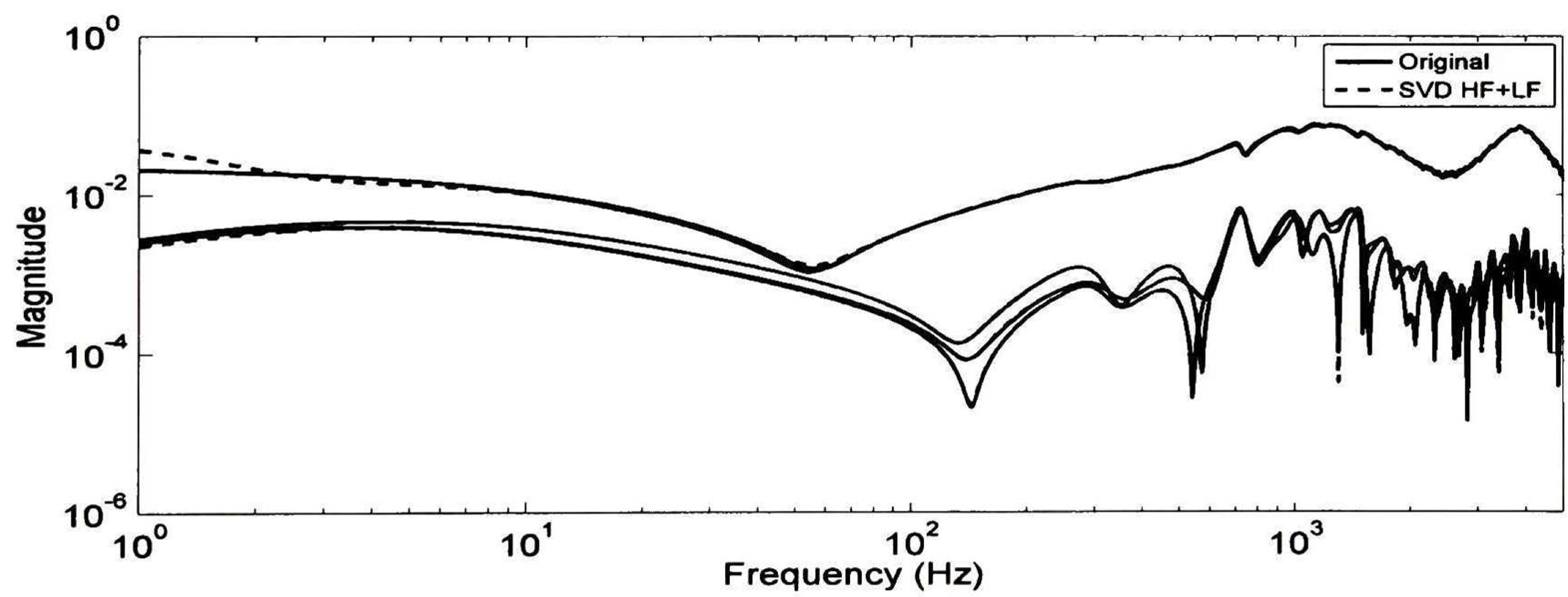

(c)

Fig. 5.8. Approximation of driving-point admittance using (a) VF, order 148, and SVD-based MOR method (b) f_{LF}, order 35, and (c) $f_{\mathrm{LF+HF}}$, order 123.

5.2.3 Time-domain response

The transient simulated in this case study is obtained by applying at $t = 0$ s the following three-phase balanced voltage input to the network of Fig. 5.7 (showing only the value for phase a):

$$u_a(t) = 66\times10^3[\sin(\omega_0 t) + 0.3\sin(3\omega_0 t) + 0.1\sin(5\omega_0 t) + 0.1\sin(7\omega_0 t) + 0.05\sin(15\omega_0 t)],$$

The computation of the transient, using a time-step of 1 μs, begins with the simulation of the 123th $f_{\mathrm{LF+HF}}$ approximation for the time subwindows $t \le t_{sw}$, with $t_{sw} = 0.01$ s; afterwards, the f_{LF} approximation is used to compute the time-domain response for the time subwindow $0.01 < t \le 0.03$ s. The transient currents by the full- and reduced-order approximations are presented in Fig. 5.9 showing a good agreement.

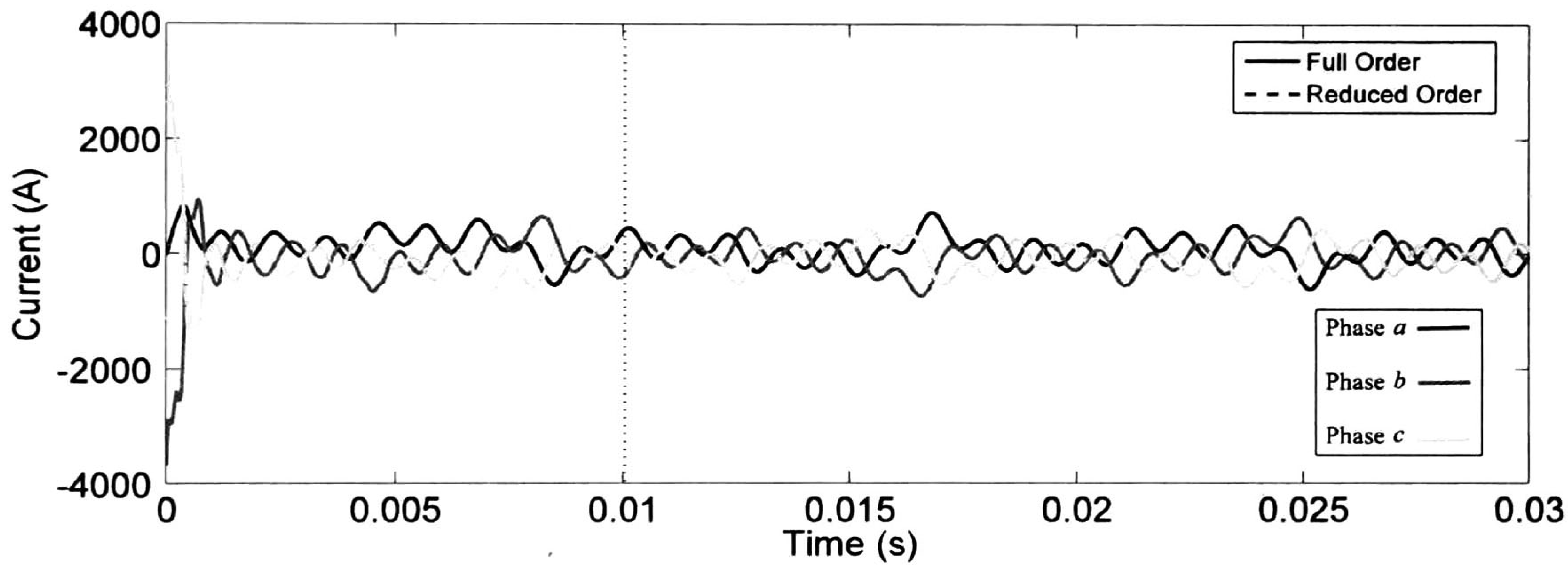

(a)

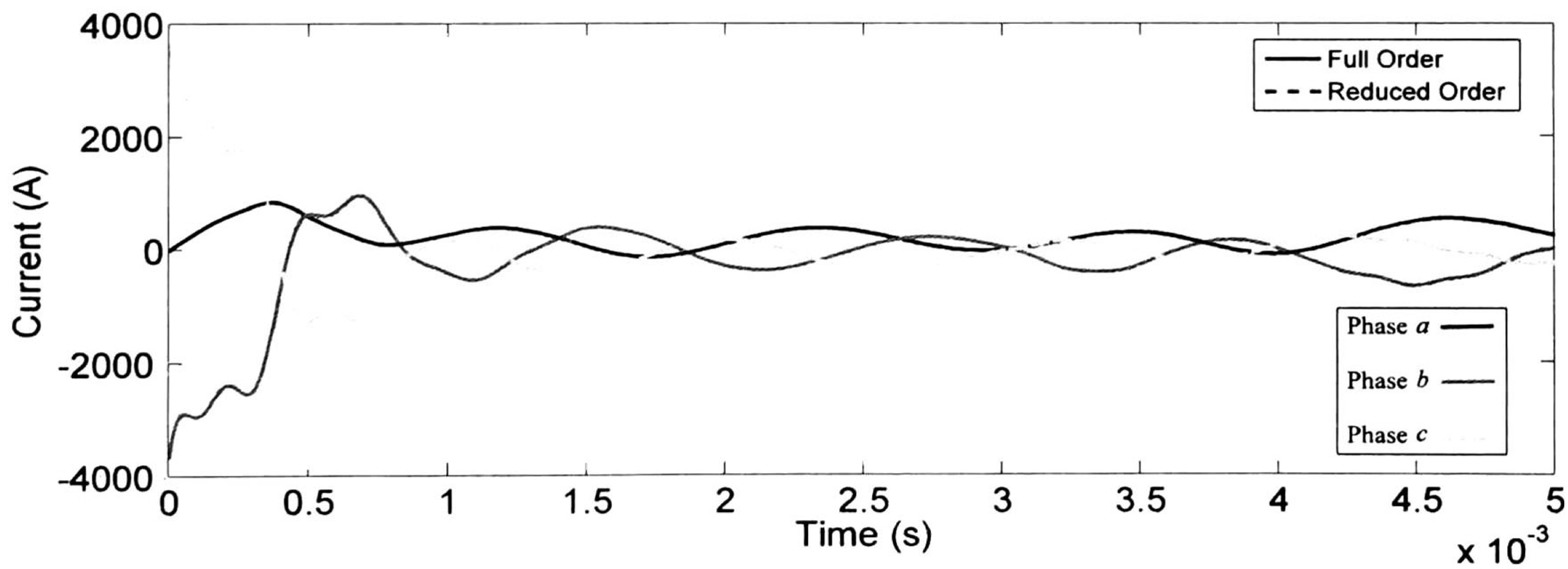

(b)

Fig. 5.9. (a) Transient waveforms by the full-order approximation given by VF and by the SVD-based MOR approximation, (b) close up.

Similarly to the single-phase case study, Table 5.7 presents different orders of approximations for the assumed Ω_{LF} and Ω_{HF} ranges. It should be mentioned that in some cases a non-passive approximation has resulted; this has been alleviated by using the passivity enforcement routine of VF.

The corresponding results of the single-phase case study, Table 5.3, are presented in Table 5.7 for the three-phase case study. Table 5.7 shows that the CPU times obtained by the proposed method are about half the required by the full-order approximation; also, the RMS error by the former is about 1%. Similar to the single-phase case, the CPU times by the SVD-based MOR method in Table 5.7 can be further reduced for smaller t_{sw} and/or larger time integration step when using f_{LF}.

The last two rows of Table 5.7 present the *rms* errors in the output transient waveforms and the CPU times, obtained by applying SVD and BR to the complete frequency range Ω. It can be observed in Fig. 5.7 that a large reduction is not achieved; from order 148 to order 139 and from 148 to 123 by application of SVD and BR to the complete frequency range, respectively. The CPU time by the 139th order system by the SVD method is comparable to the one given by VF for this case study. On the other hand, the BR method yields *rms* errors comparable to the ones given by the SVD-based MOR technique; however, the CPU time by the former is larger than the obtained by the proposed method due to BR produces a full state matrix A.

Table 5.7. RMS error in the output and CPU time for different SVD-based MOR approximations.

	r_{LF}	$r_{E_{HF}}$	r_{HF+LF}	e_{rms} (phase a)	CPU time (s)
VF	148				1.1569
SVD-based MOR	29	102	107	0.05991	0.4850
	31	118	121	0.03590	0.5474
	33	110	117	0.04975	0.5554
	35	118	123	0.01574	0.5861
SVD	139			0.02784	1.0951
BR	123			0.03450	2.6537

5.3 Conclusions

The proposed SVD-based MOR method has been validated using two different networks; the obtained results have been compared with those obtained by VF, SVD and BR considering the complete frequency range. An important feature of the proposed method is that it can use different time-steps to simulate the total time-domain response, achieving further computational savings while preserving accuracy.

6 CONCLUSIONS

6.1 Conclusions

A simple and effective SVD-based MOR technique covering a wide frequency range has been proposed and validated in this thesis. The proposed method has been applied to a single-phase network and to a three-phase network.

The obtained time-domain results show that the resultant reduced-order models reproduce with good accuracy the original response of a system, which is the main objective of MOR techniques. Since the proposed method adopts subsets of the poles given by VF, the resultant approximation retains stability properties. Also, the reduced-order model obtained by the proposed method achieves computational savings when compared to a full-order model typically obtained by VF. The performance of the proposed method also has been compared with BR and SVD-based MOR applied to the complete frequency range, showing computational superiority.

A specific application of the proposed method is MOR of a system for a narrow bandwidth aimed to analyze the system's response in that bandwidth, e.g., overvoltages, switching, lightning, DC analysis, and so on.

6.2 Future work

- To obtain an optimal time to switch between f_{LH} and f_{LF+HF}, t_{sw} to minimize CPU time.
- To develop a criterion for optimal order of the LF and HF approximations.

6.3 Publications

[1] E. Medina and A. Ramirez, "SVD-based reduced-order rational approximation on specific frequency bandwidth," ***accepted*** *in the* 2015 *North American Power Symposium (NAPS)*, paper NAPS-1131.

[2] E. Medina and A. Ramirez, "SVD-based reduced-order rational approximation for EMT analysis," ***submitted*** *for publication. IEEE Trans. Power Del.*, paper TPWRD-00783-2015.

REFERENCES

[1] B. Gustavsen and A. Semlyen, "Rational approximation of frequency domain responses by Vector Fitting," *IEEE Trans. Power Del.*, vol. 14, no. 3, pp. 1052-1061, July 1999.

[2] A. Ubolli and B. Gustavsen, "Comparison of methods for rational approximation of simulated time-domain responses: ARMA, ZD-VF, and TD-VF," *IEEE Trans. Power Del.*, vol. 26, no. 1, pp. 279-288, Jan. 2011.

[3] T. Noda, "Identification of a multiphase network equivalent for electromagnetic transient calculations using partitioned frequency response," *IEEE Trans. Power Del.*, vol. 20, no. 2, pp. 1134-1142, April 2005.

[4] U.D. Annakkage; N.K.C. Nair; Y. Liang; A.M. Gole; V Dinavahi; B. Gustavsen; T. Noda; Hassan Ghasemi; A. Monti; M. Matar; R. Iravani; J.A. Martinez, "Dynamic system equivalents: a survey of available techniques," *IEEE Trans. Power Del.*, vol. 27, no. 1, pp. 411-420, Jan. 2012.

[5] A.H. Zadegan, Ali Zilouchian, "Model reduction of large-scale systems in the neighborhood of crossover frequency," *Proc. of the 2005 IEEE International Conference on Systems, Man and Cybernetics*, pp. 3661-3666, 10-12 Oct., 2005.

[6] A. Zilouchian, P.K. Agaee, and K. Nickravesh, "Model reduction of large scaled systems via frequency-domain balanced structures," *IEEE Proc. of the American Control Conf.*, vol. 6, pp. 3873-3876, Albuquerque, NM, June 1997.

[7] A.C. Antoulas, *Approximation of large-scale dynamical systems*, Series on Advances in Design and Control, SIAM, USA, 2005.

[8] B.C. Moore, "Principal component analysis in linear systems: controllability, observability, and model reduction," *IEEE Trans. Automat. Contr.*, vol. AC-26, no. 1, pp. 17-32, Feb. 1981.

[9] Y. Hu; W. Wu; B. Zhang, "A fast method to identify the order of frequency-dependent network equivalents," *IEEE Trans. Power Del.*, early access article, 2015.

[10] A. Ramirez, "Vector fitting-based calculation of frequency-dependent network equivalents by frequency partitioning and model-order reduction," *IEEE Trans. Power Del.*, vol. 24, no. 1, pp. 410-415, Jan. 2009

[11] B. Gustavsen, "Improving the pole relocating properties of vector fitting," *IEEE Trans. Power Del.*, vol. 21, no. 3, pp. 1587-1592, July 2006.

[12] D. Deschrijver, M. Mrozowski, T. Dhaene, and D. De Zutter, "Macromodeling of multiport systems using a fast implementation of the vector fitting method", *IEEE Microwave and Wireless Components Letters*, vol. 18, no. 6, pp. 383-385, June 2008.

[13] B. Gustavsen, "Computer code for rational approximation of frequency dependent admittance matrices," *IEEE Trans. Power Del.*, vol. 17, no. 4, pp. 1093-1098, Oct. 2002.

[14] E. Medina and A. Ramirez, "SVD-based reduced-order rational approximation on specific frequency bandwidth," *Accepted in the* 2015 *North American Power Symposium (NAPS)*, paper NAPS-1131.

[15] The Mathworks, Matlab R2012b.

[16] A. Semlyen and B. Gustavsen, "Vector Fitting by pole relocation for the state equation approximation of nonrational transfer matrices," *Circuits Systems Signal Process*, vol. 19, no. 6, pp. 549-566

[17] E. Hairer, C. Lubich, and G.Wanner, *Geometric Numerical Integration*, 2nd Ed., Springer, 2006.

[18] M. Matar and R. Iravani, "A modified multiport two-layer network equivalent for the analysis of electromagnetic transients," *IEEE Trans. Power Del.*, vol. 25, no. 1, pp. 434-441, Jan. 2010.

[19] H.W. Dommel, "Electromagnetic Transients Program Reference Manual (EMTP Theory book)," Bonneville Power Administration, Portland, Ore., August 1986.

APPENDIX A

Network equivalent, case study 1

To calculate the driving-point admittance of case study 1, all overhead lines and underground cables are represented by their two-port network models as shown in Fig. 6.1 [19].

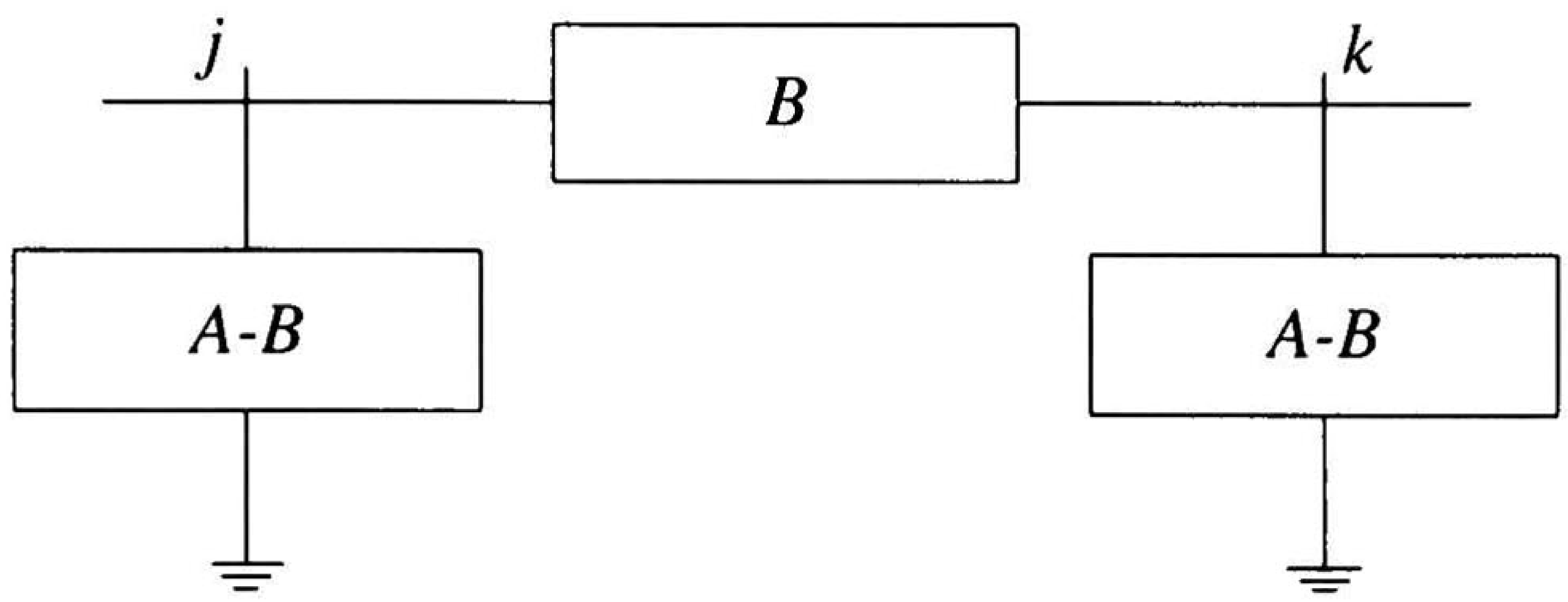

Fig. A.1 Line/cable admittance two-port network representation.

where:

$$A = Y_c \coth(\gamma l), \tag{A.1}$$

$$B = Y_c \operatorname{csch}(\gamma l), \tag{A.2}$$

Y_c and γ, given in (A.3) and (A.4), represent characteristic admittance and propagation function respectively; l represents the length.

$$Y_c = \sqrt{\frac{Y}{Z}}, \tag{A.3}$$

$$\gamma = \sqrt{ZY} \tag{A.4}$$

Based on the above mentioned line/cable representation and load admittances, the nodal admittance matrix (Y_{BUS}) is calculated as

$$I = Y_{BUS} V. \tag{A.5}$$

where

$$I = [i_s \quad 0 \quad 0 \quad 0 \quad 0 \quad 0 \quad 0 \quad 0 \quad 0 \quad 0]^T \tag{A.6}$$

$$V = [V_1 \quad V_2 \quad V_3 \quad V_4 \quad V_5 \quad V_6 \quad V_7 \quad V_8 \quad V_9 \quad V_{10}]^T \tag{A.7}$$

$$Y_{BUS} = \begin{bmatrix} Y_{11} & Y_{12} \\ Y_{21} & Y_{22} \end{bmatrix} \tag{A.8}$$

The driving point admittance is obtained as

$$H = Y_{11} - Y_{12} Y_{22}^{-1} Y_{21}, \tag{A.9}$$

where:

$$Y_{11} = [A_{UC}], \tag{A.10}$$

$$Y_{12} = [-B_{UC} \quad 0 \quad 0 \quad 0 \quad 0 \quad 0 \quad 0 \quad 0 \quad 0], \tag{A.11}$$

$$Y_{21} = Y_{12}^{T}, \tag{A.12}$$

$$Y_{22} = \begin{bmatrix} A_{UC} + A & -B & 0 & 0 & 0 & 0 & 0 & 0 & 0 \\ -B & A_{UC} + A + Y_l & -B_{UC} & 0 & 0 & 0 & 0 & 0 & 0 \\ 0 & -B_{UC} & A_{UC} + 2A + Y_l & -B & -B & 0 & 0 & 0 & 0 \\ 0 & 0 & -B & 3A + Y_l & 0 & -B & -B & 0 & 0 \\ 0 & 0 & -B & 0 & 3A + Y_l & 0 & 0 & -B & -B \\ 0 & 0 & 0 & -B & 0 & A & 0 & 0 & 0 \\ 0 & 0 & 0 & -B & 0 & 0 & A & 0 & 0 \\ 0 & 0 & 0 & 0 & -B & 0 & 0 & A & 0 \\ 0 & 0 & 0 & 0 & -B & 0 & 0 & 0 & A \end{bmatrix}. \tag{A.13}$$

In (A.10) to (A.13), A_{UC} and B_{UC} correspond to the UC parameters while A and B are the parameters of the ten identical overhead lines parameters.

Appendix B

Network equivalent, case study 2

The computation of the three-phase driving-point admittance of the network shown in Fig. 5.7, is carried out similarly to the single-phase case. For the three-phase case, the two-port network model of the overhead lines and underground cables involve matrices of dimensions 3×3, represented by

$$A = Y_c \coth(\gamma l), \tag{B.1}$$

$$B = Y_c \operatorname{csch}(\gamma l), \tag{B.2}$$

where Y_c and γ are calculated as shown in (B.3) and (B.4) respectively.

$$Y_c = Z^{-1}\sqrt{ZY} \tag{B.3}$$

$$\gamma = \sqrt{ZY} \tag{B.4}$$

Similarly to the single-phase case, the nodal admittance matrix (Y_{BUS}) is given by

$$I = Y_{BUS} V. \tag{B.5}$$

where

$$I = [I_s \quad 0 \quad 0 \quad 0 \quad 0 \quad 0 \quad 0 \quad 0 \quad 0 \quad 0 \quad 0]^T \tag{B.6}$$

$$V = [V_1 \quad V_2 \quad V_3 \quad V_4 \quad V_5 \quad V_6 \quad V_7 \quad V_8 \quad V_9 \quad V_{10} \quad V_{11} \quad V_{12}]^T \tag{B.7}$$

$$Y_{BUS} = \begin{bmatrix} Y_{11} & Y_{12} \\ Y_{21} & Y_{22} \end{bmatrix}. \tag{B.8}$$

Elements of (B.8) are given by

$$Y_{11} = [A_{UC}], \tag{B.9}$$

$$Y_{12} = [-B_{UC} \quad O \quad O \quad O \quad O \quad O \quad O \quad O \quad O \quad O \quad O], \tag{B.10}$$

$$Y_{21} = Y_{12}^T, \tag{B.11}$$

$$
Y_{22} = \begin{bmatrix}
A_{1c} + A_1 & -B_1 & O & O & O & O & O & O & O & O & O \\
-B_1 & A_1 + A_2 + Y_1 & -B_2 & O & O & O & O & O & O & O & O \\
O & -B_2 & A_2 + A_3 + A_4 + Y_2 & -B_4 & -B_3 & O & O & O & O & O & O \\
O & O & -B_4 & A_4 + A_7 + Y_4 & O & O & -B_7 & O & O & O & O \\
O & O & -B_3 & O & A_3 + A_5 + A_6 + Y_3 & -B_6 & O & -B_5 & O & O & O \\
O & O & O & O & -B_6 & A_6 + A_9 + Y_6 & O & O & -B_9 & O & O \\
O & O & O & -B_7 & O & O & A_7 + Y_7 & O & O & O & O \\
O & O & O & O & -B_5 & O & O & A_5 + A_8 + Y_5 & O & -B_8 & O \\
O & O & O & O & O & -B_9 & O & O & A_9 + Y_9 & O & O \\
O & O & O & O & O & O & O & -B_8 & O & A_8 + A_{10} + Y_{10} & -B_{10} \\
O & O & O & O & O & O & O & O & O & -B_{10} & A_{10} + Y_{10}
\end{bmatrix}, \quad \text{(B.11)}
$$

where O is a matrix of dimensions 3×3, containing only 'zeros' as elements.

Finally, the driving point admittance for the three-phase case is calculated as

$$
H = Y_{11} - Y_{12} Y_{22}^{-1} Y_{21}. \quad \text{(B.12)}
$$

CENTRO DE INVESTIGACIÓN Y DE ESTUDIOS AVANZADOS DEL I.P.N.
UNIDAD GUADALAJARA

El Jurado designado por la Unidad Guadalajara del Centro de Investigación y de Estudios Avanzados del Instituto Politécnico Nacional aprobó la tesis

Reducción de Orden de Aproximaciones Racionales para Análisis de Transitorios Electromagnéticos Utilizando Descomposición en Valores Singulares

del (la) C.

Edgar Yitzhak MEDINA LARA

el día 16 de Octubre de 2015.

Dr. José Manuel Cañedo Castañeda
Investigador CINVESTAV 3C
CINVESTAV Unidad Guadalajara

Dr. Amner Israel Ramírez Vázquez
Investigador CINVESTAV 3C
CINVESTAV Unidad Guadalajara

Dr. José de Jesús Chávez Muro
Coordinador del programa de graduados e investigación en ingeniería eléctrica
Instituto Tecnológico de Morelia